

AD-A277 430

AGE

Approved for public release;
distribution unlimited.

1. AGENCY USE ONLY (Leave blank)

2. REPORT DATE

3. REPORT TYPE AND DATES COVERED

ANNUAL 1 Dec 92 TO 30 Nov 93

4. TITLE AND SUBTITLE

FINITE-ELEMENT MODELING OF THE BLOCKAGE AND SCATTERING
OF LG PROPAGATION

F49620-93-1-0073

61102F

2309

AS

5. AUTHOR(S)

Dr Yu-chiung Teng

6. PERFORMING ORGANIZATION NAME(S) AND ADDRESS(ES)

Dept of Engineering & Applied Sciences
Columbia University
842 S.W. Mudd
New York, NY 10027

AFOSR-TR- 94 0099

7. MONITORING AGENCY NAME(S) AND ADDRESS(ES)

AFOSR/NL
110 DUNCAN AVE SUITE B115
BOLLING AFB DC 20332-0001

8. MONITORING AGENCY NAME(S) AND ADDRESS(ES)

94-09422



Dr Dickinson

9. SUPPLEMENTARY NOTES

DTIC
ELECTE
MAR 28 1994
S B D

10. DISTRIBUTION AVAILABILITY STATEMENT

Approved for public release;
distribution unlimited

11. DISTRIBUTION CODE

12. ABSTRACT (Maximum 200 words) The problem of Lg wave blockage is being investigated using finite element models of island margin, basin, and basin with an uplifted Moho to simulate wave propagation across the Barents Sea basin. Results from the first year follow. The efficiency of the crust as a Lg wave guide strongly depends on the frequency content of an impulsive source. The effects of a basin on Lg propagation also depends on the basin width and the velocity contrast between the sedimentary basin and the surrounding granitic/basaltic crust. For a high velocity contrast, the Lg wave form is significantly lengthened. The presence of an uplifted Moho alone does not appear to have a major blockage effect on Lg wave propagation. The finite element codes with the fast execution algorithm prove to be well suited as tools for the modeling purposes intended in this research.

13. SUBJECT TERMS

15. NUMBER OF PAGES

16. PRICE CODE

17. SECURITY CLASSIFICATION
OF REPORT

(U)

18. SECURITY CLASSIFICATION
OF THIS PAGE

(U)

19. SECURITY CLASSIFICATION
OF ABSTRACT

(U)

20. LIMITATION OF ABSTRACT

(U)

AD-A277 430-5500

DISTRIBUTION

Standard Form 298-100 Rev. 1-79
Prescribed by ANSI Z39-18-1983

94 3 25 120

**ANNUAL REPORT
TO
THE AIR FORCE OFFICE OF SCIENTIFIC RESEARCH**

CONTRACT NO: F49620-93-0073

**FINITE-ELEMENT MODELING OF THE BLOCKAGE AND
SCATTERING OF Lg WAVE PROPAGATION**

Yu-Chiung Teng and John T. Kuo
Aldridge Laboratory of Applied Geophysics
Henry Krumb School of Mines
Columbia University, New York, New York 10027

December, 1993

TABLE OF CONTENTS

ABSTRACT	1
INTRODUCTION	4
RELEVANCE TO THE GOALS FOR DETECTION OF UNDERGROUND NUCLEAR TESTS	6
RESEARCH ACCOMPLISHED	8
FUTURE WORKS	18
CONCLUSIONS	19
FIGURES	20
REFERENCES	53

Accession For	
NTIS GRA&I	<input checked="" type="checkbox"/>
DTIC TAB	<input type="checkbox"/>
Unannounced	<input type="checkbox"/>
Justification	
By _____	
Distribution/	
Availability Codes	
Dist	Avail and/or Special
A-1	

ABSTRACT

This report constitutes the annual report to the Air Force Office of Scientific Research under the Contract F49620-93-1-0073 which commenced on December 1, 1993, for the research project on the Blockage and Scattering of Lg Waves.

The objective of the project is to investigate by means of finite-element modeling of the problem of blockage and scattering of Lg wave propagation due to lateral crustal heterogeneities, particularly from presumed explosions at test sites of Novaya Zemlya across the Barents Sea to ARCESS, NORESS and Graefenburg. This research project is to provide not only a contribution to a more quantitative understanding of the blockage and scattering of Lg propagation, but also an enhancement of the capabilities of the use of Lg amplitude discrimination as event identification and yield estimation.

As a first step, the effects of the blockage and scattering by a basin of various widths filled with sediments on the Lg propagation have been investigated. A series of anti-plane strain (SH) finite-element models, simulating two relevant geological provinces for the great-circle paths of the posed problem have been constructed, including, (1) the Island Margin Model, (2) the Basin Model, and (3) the Basin and Crust-Pinch Model with an uplifted Moho. Three different center-frequencies, 0.167, 0.334, and 0.667 Hz of an impulsive source are used in the excitation of the Lg waves.

During the first year of the Contract, we found that:

1. the problem of Lg wave propagation in a complex, laterally inhomogeneous wave guide, such as in the present case of simulating the propagation path from Novaya Zemlya through the Barents Sea, can be accomplished by multi-

steps. This multi-step methodology developed here promises to handle even larger dimension models than we studied here, without degrading the accuracy of numerical results. The multi-steps we suggested are, namely, that:

- (a) an impulsive source be placed in the Island Margin Model to obtain the seismic response everywhere in the model;
 - (b) the output of the seismic response, in our case we choose BB' , be used as an input source to drive the Basin Model, and the Basin and Crust Pinch Model.
2. the presence of an idealized basin has an effect on the blockage of the L_g wave propagation. The manner of blockage is of frequency-dependent, of width of the basin and velocity contrast between the sedimentary basin and the surrounding granitic/basaltic crust.
 3. the presence of an uplifted Moho alone without a basin seems only to have a minor effect on the L_g wave propagation.
 4. an unusual event which is generally not observed on the surface has been observed in the upper mantle for the Island Margin Model. The event is attributed to the multi-reflected in the margin and the transmitted through the upper mantle.
 5. the velocity contrast between the sediments in the basin and the surrounding granitic/basaltic crust plays a vital role on determining the characteristics of both S_n and L_g , and particularly on the scattering, development and attenuation of the L_g waves. For a high velocity contrast, the wave train of the L_g waves is lengthened drastically.
 6. the energy envelop of the so-called L_g waves often contains the arrival of the direct S waves.

As the project has been extended for the second year, systematic studies have been contrived to gain more basic understanding of the mechanism of the blockage of Lg wave propagation in a laterally inhomogeneous earth, specifically simulating the Lg propagation from Novaya Zemlya through the Barents Sea, the Baltic shield and the European continent.

INTRODUCTION

The principal objective of this research project is to improve basic knowledge of the Lg propagation and its mechanisms from presumed explosions at test sites of Novaya Zemlya across the Barents Sea to ARCESS, NORESS, and Graefenburg.

The monitoring of underground nuclear explosions, unlike the monitoring of atmosphere and underwater nuclear tests, can be detected with relatively high degree of confidence. It remains a critical part of the global verification system. Seismology provides a technical means for monitoring underground nuclear testing. By investigating seismograms and knowing the general properties of the propagation paths of teleseismic body and surface waves (recorded at a distance over 2,000 km), and of regional waves (such as P_n , P_g , S_n , and Lg recorded at a distance less than 2,000 km), seismologists are able not only to calculate the distance to the seismic event and to deduce the type of motion to excite the waves, but also to make yield estimation and event identification based on Lg amplitudes.

The efficiency of Lg wave propagation highly depends on the structure and lithology of geological provinces along its propagation path. Ruzaiquin et al. (1977) attributed the inefficient propagation of Lg in the Tibetan Plateau to the variation of crustal thickness, where an unusual thickness of crust is present. Kennett et al. (1985) suggested that the Lg propagation across the Norwegian Sea might be suffered from a blockage of regional crustal thickening beneath a graben structure of a basin. Kadinsky-Cade et al. (1981), Ni and Barazangi (1983), and others used the efficiency of Lg propagation as a method for mapping tectonic boundaries of variable thicknesses. Baumgardt (1985, 1990a), along the same vein, attributed to the partial blockage of Lg propagation in Eurasia by the presence of the Ural Mountains from Semipalatinsk test site in eastern Kazakh to ARCESS.

Baumgardt (1990a, 1990b, 1991) found that the Lg waves are almost completely missing at ARCESS and very poorly recorded at NORESS, while "the Lg energy of some kind appears to get through to the Graefenburg array at about the time expected for on-time Lg." It is apparent that variations of Lg amplitudes are closely associated with the problem of blockage and scattering of Lg waves along its propagation path.

Nevertheless, there is still a great deal of uncertainties in basic understanding of the generation and propagation of Lg waves in a laterally heterogeneous crust that is relevant to yield estimation and event identification for nuclear test detection. One of the problems of Lg propagation in the earth crust has been the blockage and scattering along its propagation path, and the mechanisms affecting its propagation.

Analytic solutions to the Lg wave propagation in such a laterally heterogeneous crust are generally intractable. It appears that discretization methods such as the finite-element method can be profitably applied to simulate Lg propagation in laterally heterogeneous media. The finite-element method (FEM) is a numerical procedure for solving very general partial differential equations, such as the full elastic wave equations. It can accurately simulate the propagation of transient elastic waves through complex geologic structures and, otherwise, heterogeneous media.

During the first year of the AF Contrac F'9620-93-0073, we have studied both forward- and backward-traveling Lg waves for each of the trapped modes in a laterally heterogeneous, realistic geogical structure to give a full representation of the wave field by means of the FEM. Since the method calculates the elastic components of ' displacement at every nodal point on a fine grid which discretizes the subsurface structure, the results produce not only the complete synthetic seismogram at any nodal

point but also an image of the displacement wave field as it is propagated through the Earth, that is, a wave field image, or a snapshot. By correlating the snapshots with surface records, individual seismic arrivals can be identified on a seismogram, in terms of the blockage and scattering of Lg waves due to a variety of obstacles.

We used our time-domain-finite-element computer codes, with fast computation algorithms developed at Aldridge and systematically investigated the effects of lateral crustal heterogeneities on Lg wave propagation.

A series of anti-plane strain (SH waves) finite-element models have been constructed to simulate the evolution and blockage of Lg waves by means of a variety of relevant geological provinces extending from an Island Margin through a basin and crust-pinch structure to a normal crust.

RELEVANCE TO THE GOALS FOR DETECTION OF UNDERGROUND NUCLEAR TESTS

This research is motivated by the works of a number of investigators, who suggested that the blockage of Lg wave propagation in the continents primarily due to lateral crustal heterogeneities, and particularly by a series of papers by Baumgardt (1985, 1987, 1990a, 1990b, and 1991), addressing the problem of the blockage and scattering of the Lg wave propagation from the Russian test sites to the Scandinavian arrays due to the presence of the Barents Sea Basin. A more quantitative understanding of the blockage and scattering of Lg propagation and their mechanisms from Novaya Zemlya to the regional arrays may enhance the use of Lg amplitude discrimination as event identification and yield estimation elsewhere.

The 1989 announced intention of the Soviets to shift their underground nuclear testing activities from the test site near Semipalatinsk in western Kazakh to the Arctic island of Novaya Zemlya, made the study of regional Lg propagations from Novaya Zemlya to the Scandinavian arrays and Graefenburg relevant. The distances from Novaya Zemlya to the regional arrays, ARCESS and NORESS are 10° and 20° respectively, and to Graefenburg is 29.5° . Ther we have accumulated a great deal of seismic data. Although our initial models will be somewhat simplified, they are and essential to gain basic understanding of the blockage and scattering of Lg propagation across the laterally heterogeneous crust, and then to be compared with actual data.

RESEARCH ACCOMPLISHED

I. GEOLOGICAL STRUCTURE

Gramberg (1988) and Clarke and Rachlin (1990) provided fairly comprehensive geological maps of the Barents Sea and its vicinities, including Novaya Zemlya, the Kola Peninsula, Cheshkaya Bay, just above the Arctic Circle. Presumably, on the basis of the geological information given, Baumgardt (1990b) has constructed a NW-SE geological cross section (Figure 1). Similar geological cross sections along the great-circle paths from Novaya Zemlya to ARCESS, NORESS and Graefenburg, in which we are particularly interested, can be approximately constructed. Thus, from Novaya Zemlya to the Scandinavian arrays, namely ARCESS and NORESS, and to Graefenburg, the great-circle paths of Lg essentially traverse major geological provinces, (1) the island margin with variable crust thicknesses (from Novaya Zemlya to the Barents Sea), (2) the basin with variable width, depth and sediments (the Barents Sea Basin), (3) the shield margin (from the Barents Sea to the Baltic shield), and finally (4) the shield and European continent with variable crustal thickness and lithology (from the Baltic shield to Graefenburg).

The Barents Sea Basin can be characterized by variations of crustal thickness with sediment accumulation as much as 15 km, and by missing of a granitic layer. This structure is based on low in magnetic anomalies caused by the missing of granitic layer and on high in gravity anomalies caused by the elevated Moho. As reported, the granitic layer in the adjacent province is characterized by P wave velocities on the order of 6.0 to 6.5 km/sec, and S wave velocities 3.46 to 3.75 km/sec (Clarke and Rachlin, 1990). The sediments assume P wave velocities from 3.9 to 5.5 km/sec, and, correspondingly, S wave velocities 2.2 to 3.17 km/sec (Baumgardt, 1990a, 1991).

The basaltic layer assumes P wave velocities from 6.5 to 6.8 km/sec and S wave

velocities from 3.47 to 3.63 km/sec.

The upper mantle is assumed to be normal with P wave velocities ranging from 8.1 to 8.2 km/sec, and S wave velocities of 4.6 to 4.7 km/sec.

The density of the sediments are taken to be 2.2 to 2.5 gm/cm³; that of granitic layer to be 2.67; that of basaltic layer to be 3.0 in the crust; and that of ultrabasic rocks in the upper mantle to be 3.27.

II. MODEL CONSTRUCTION

For the first year, we restrict our investigation for the great-circle path of Lg traverse the first two major geological provinces, namely (1) the Island Margin Model, and (2) the Basin Model, and (3) the Basin and Crust and Pinch Model. Two basic models have been constructed to simulate the geological structures along the path from the former USSR nuclear test sites of Novaya Zemlya to the Barents Sea. The island margin portion of both the two basic models is identical. The Barents Sea portion of the two basic models is different by the interface between the lower crust and the upper mantle,

(1) Model I, the Barents Sea is represented by an idealized sedimentary basin which occupies the upper crust. The interface of the lower crust and the upper mantle is flat (Figure 2-(a)).

(2) Model I, the Barents Sea is represented by a sedimentary basin, which again occupies the upper crust. The lower crust is intruded by the Moho uplift of the upper mantle into the crust (figure 2-(b)).

An impulsive, transient source of the first derivative of Gaussian type forcing

functions is placed on the island marked by '**'.

In order to avoid the artificially terminated effect of the left boundary of the island margin at BB' on the FEM, an Island Margin Model is constructed as follows:

(A) The Island Margin Model

The Island Margin model is characterized by a sloping interface of the crusts and the upper mantle. The source is located on the island side of the model (Figure 3-(a)). The S wave velocities of the granitic/basaltic (averaged) layer and the upper mantle are taken to be 3.51 km/sec and 4.7 km/sec, respectively. The source are simulated by an impulsive explosion with three different center frequencies, namely, 0.167 Hz, 0.334 Hz, and 0.667 Hz to investigate the effect of the source frequency contents on the Lg wave propagation. The right artificially terminated boundary is placed on the other side of of the island by AA'; the left artificially terminated boundary is placed about 100 from BB'.

(B) The Basin and Crust-Pinch Models

We consider a series of models with two different basin widths of 150 km and 250 km, but with a fixed center frequency of the source 0.334 Hz. The seismic waves, as shown in Figure 5-(b), so generated by the impulsive source of the island margin received at the BB' BB' in Figure 3-(a) are used as the input waves at BB' for the basin, and basin and crust-pinch models to provide the continuity, as if the waves propagated from the impulsive source on the island. (Figure 3-(b) or Figure 3-(c).)

The geophysical parameters of these models are as follows: The basin models as shown in Figure 3-(b), with a basin width = 150 km; shear velocities for: granitic/basaltic (averaged) = 3.51 km/sec, and the upper mantle = 4.7 km/sec.

(1) for sediments = 3.51 km/sec;

(2) for sediments = 2.70 km/sec;

(3) for sediments = 2.20 km/sec;

The basin and crust-pinch models with an uplift of the Moho as shown in Figure 3-(c), with

(4) the same parameters as case (1).

(5) the same parameters as case (2).

(6) the same parameters as case (3).

The basin models as shown in Figure 3-(b), with a different basin width, i.e., a basin width = 250 km; shear velocities for: granitic/basaltic (averaged) = 3.51 km/sec; and the upper mantle = 4.7 km/sec.

(7) for sediments = 3.51 km/sec;

(8) for sediments = 2.70 km/sec;

(9) for sediments = 2.20 km/sec;

The basin and crust pinch models with an uplift of the Moho as shown in Figure 3-(c), with a basin width = 250 km; shear velocities for : granitic/basaltic (averaged) = 3.51 km/sec; and the upper mantle = 4.7 km/sec.

(10) the same parameters as case (7).

(11) the same parameters as case (8).

(12) the same parameters as case (9).

III. RESULTS

Figures 4-(a), 4-(b), 4-(c) are the synthetic seismograms obtained from Model A by using 0.167 Hz, 0.334 Hz, and 0.667 Hz, sources respectively. The synthetic seismograms obtained from Model B by the source of a center frequency 0.334 Hz are shown in Figures 6-(a) to 6-(f) (corresponding to Case 1 to Case 6), Figures 7-(a) to 7-(f) (corresponding to Case 7 to Case 12). We have also calculated two series

of models with the same geophysical parameters as Case 7 to Case 12, but with the 0.167 Hz center frequency source (as shown in Figure 5-(a)), and the 0.667 Hz source (as shown in Figure 5-(c)), respectively. We assign the six cases with 0.167 Hz source as Case 13 to Case 18 with the corresponding synthetic seismograms as shown in Figures 8-(a) to 8-(f), and the six cases with 0.667 Hz source as Case 19 to Case 24 with the corresponding synthetic seismograms as shown in Figures 9-(a) to 9-(f).

It is expected that a seismogram would have typically regional waveforms, with relatively sharp P_n onsets, an emergent arrival corresponding to the S_n onset, and the strong Lg arrivals. However, the present finite element numerical results, of course, do not generate the P_n waves, since we treat it as an anti-plane strain problem for the Lg waves.

The arrivals of both the S_n and Lg are clearly shown in Figures 4-(b) and 4-(c), on the finite element synthetic seismograms due to an impulsive source with center frequencies of 0.334 Hz and 0.667 Hz, respectively. The arrival of S_n for an impulsive source with a center frequency 0.167 Hz as shown in Figure 4-(a) is a broader event because of a long duration of the pulse. In the distance range investigated, 10 - 250 km, the so called Lg begins with the direct arrival of S, i.e. SH. In another word, the direct S is often included in the energy envelop of the Lg waves.

In order to illustrate the crustal wave guide phenomena for the energy of the Lg and S_n waves, we have calculate seismograms as a function of depth from the crust through the upper mantle. Figures 5-(a), 5-(b) and 5-(c) show the responses at BB' (see Figure 3-(a)), corresponding to the center frequencies of the source, 0.167, 0.334, and 0.667 Hz, respectively. The energy is virtually trapped in the crust to make it a nearly perfect wave guide for the Lg wave generation and propagation. However, for lower frequencis, there is a leakage of energy from the crust to the upper mantle. As

the interface of the crust and the upper mantle is placed at a depth of 30 km with the center frequency of the source 0.667 Hz, (Figure 5-(C)) shows that the energy of Lg is all confined to the crust. For a lower center frequency such as shown in Figure 5-(a) with a center frequency of 0.167 Hz, the energy of Lg in the subsurface is transmitted through the upper mantle as deep as a half of the crustal thickness to a depth of 45 km, that in Figure 5-(b) with a center frequency of 0.334 Hz, the energy of Lg is transmitted through the upper mantle at a depth of about 38 km, or a quarter of the crustal thickness. Therefore, the crustal wave guide for the Lg waves for a variable thickness of the crust such as for the margin model is of frequency dependent.

Figures 5-(a),(b), (c) show an interesting event which is generally not observed on the surface, that is the arrival of an event in the upper mantle ahead of S_n in the crust. These arrivals are interpreted as a multi-reflected in the margin and then refracted into the upper mantle, denoted by S_{clR} , where 'cl' stands for reflected in the crust and 'R' stands for refracted and transmitted through the upper mantle. As a matter of fact, the amplitude of S_{clR} increases as a function of depth as observed at a distance of 250 km clearly shown in Figures 5-(a), (b), and (c). These arrivals are less multi-reflections in the margin. The average envelopes of the Lg waves are broader for the source with lower frequencies.

The responses, as shown in Figure 5-(b), are used as the input source at BB' in the Basin Model (see Figure 3-(b)). Figure 6-(a) shows the synthetic seismograms obtained from the model with the basin replaced by the granitic/basaltic (averaged) velocity of 3.51 km/sec, that is, a layer of granitic/basaltic (averaged) over the upper mantle. Shear wave reverberation in the averaged granitic/basaltic layer is clearly shown to produce an expected group velocity for Lg of approximately 3.5 km/sec, and for S_n waves with a group velocity of 4.4 km/sec.

Nevertheless, Figures 6-(b) and 6-(c) are the results obtained from the Basin model (with basin width = 150 km as in Figure 3-(b)) with two different sediment velocities, 2.7 km/sec and 2.2 km/sec, excited by the input waves at BB' in Figure 5-(b). In both cases, in addition to the arrivals of S_n and Lg observed from 20 - 400 km, there are scattering events from the two limbs of the basin clearly shown at the locations between the source and the left limb of the basin as marked by the dashed lines. The reflections come later but stronger for the basin velocity of 2.2 km/sec case (Figure 6-(c)) due to a higher contrast of velocity between the crust and the sedimentary in the basin in comparison with that of the 2.7 km/sec case (Figure 6-(b)). In the locations closer to the source, the main features as shown in Figure 6-(b) and 6-(c), are the emergent arrivals followed by the distinct Lg arrivals. While at the locations adjacent to or beyond the left limb of the basin, the Lg waves have been developed into a complicated long tremor (or codas) with the amplitude diminish with time. With the presence of basin, the synthetic seismograms also show the delay of the arrivals of Lg waves.

Figure 7-(a) and Figure 6-(a) are virtually identical. Figures 7-(b) and 7-(c), which are corresponding to the cases of Figures 6-(b) and 6-(c) but with a wider basin width of 250 km, show all the essential wave characteristics as revealed in Figures 6-(b) and 6-(c), except the laterally scattered waves from the limbs of the basin are delayed by traveling the additional width of the basin. These scattered waves are also separated into the S_n and Lg arrivals.

Figures 6-(d) and 7-(d) are the synthetic seismograms for the cases with an uplifted Moho corresponding to the Moho-uplift width of 150 km and 250 km respectively, but without the presence of the basin. With the input waves of a center frequency 0.334 Hz, the wavelength is still too short to have the effect of the uplift of the Moho on the Lg propagation observed on the surface. The arriving times for both S_n and

Lg is earlier and S_n are stronger than those for the cases without a Moho-uplift.

Figures 6-(e) and 7-(e) show the synthetic seismograms for the basin and Moho uplifted model (Figure 3-(c)) otherwise identical configuration as in Figures 6-(d) and 7-(d), except the width of the basin being 150 km and 250 km, respectively. The scattered waves due to the limbs of the basin are clearly observed in both Figures 6-(e) and 7-(e). Both S_n and Lg are well developed in both the cases of the width of the basin 150 km and of that 250 km, in the distances from 20 - 400 km from the source location. However, in the case of the width of the basin 250 km, the amplitude of the Lg decays more rapidly than that in the case of the width of the basin 150 km. The phenomenon of the Lg blockage by the basin in the case of the basin alone model is clearly shown beyond the observing distance 300 km for the case with the width of the basin 250 km (Figure 7-(c)); and beyond the observing distance 200 km for the case with the width of the basin 150 km (Figure 6-(c)). In the case of the basin width 150 km, the amplitude of the Lg, decays in the distance from 220 km to 340 km, and then regains beyond 340 km. These observations clearly demonstrate the phenomena of the blockage of the Lg waves by the presence of the low velocity sedimentary basin. Now we examine Figures 6-(f) and 7-(f), which are the Basin Model with the identical structural and velocity parameters, but the width of the basin being 150 km and 250 km, respectively. In Figures 6-(f) and 7-(f), again the scattered waves due to the limbs of the basin come later but stronger due to a higher contrast of velocity between crust and the sedimentary in the basin in comparison with those in Figures 6-(e) and 7-(e).

Although an uplifted Moho appears to have only minor effects on the Lg propagation for the center frequency 0.335 Hz of the source investigated, the uplifted Moho associated with the basin does have considerable effects on the Lg propagation. We find that:

(1) The larger the velocity contrast between the basin sediments and the surrounding granitic/basaltic crust is, the stronger is the scattering, and the longer are the delay and attenuation of the Lg waves;

(2) The wider the basin width, the longer is the delay of the Lg waves.

For detailed investigation of the effects of the center frequency of the impulsive source and the velocity of the sedimentary basin on the Lg waves, we, in addition, have calculated the cases for the center frequencies of 0.167 Hz and 0.667 Hz of the source for:

(1) A layer case without Moho uplifted and with Moho uplifted with a basin velocity of 3.51 km/sec (Figures 8-(a), 8-(d), and Figures 9-(a), 9-(d), respectively);

(2) A basin model without Moho uplifted and with Moho uplifted, with a basin velocity of 2.7 km/sec (Figure 8-(b), 8-(e), and Figures 9-(b), 9-(e), respectively);

(3) A basin model without Moho uplifted and with Moho uplifted, with a basin velocity of 2.2 km/sec (Figure 8-(c), 8-(f), and Figures 9-(c), 9-(f), respectively);

The essential features of S_n and Lg and the scattered S_n and Lg for the center frequencies 0.167 Hz and 0.667 Hz of the source above are precisely similar to the cases of those for the center frequency 0.334 Hz of the source for these cases (see corresponding Figures 7-(a) to 7-(f)), viz.,

1. The emergent arrival corresponding to the S_n onset;
2. A distinct strong Lg arrival at the distances closer to the source;
3. At the locations adjacent to or beyond the left limb of the basin, the Lg waves are spread out into long codas with their amplitude diminishing with time;
4. The larger the velocity contrast between the basin sediments and the surround-

ing granitic/basaltic crust is, the stronger is the scattering, and more the delay and the attenuation of the Lg waves,

5. The higher the frequency of the source, the more attenuated are the S_n arrivals.

The effects of the velocity of sedimentary basin on both the development and appearance of S_n , and Lg are substantial. When the contrast of the velocities between the basin and the surrounding granitic/basaltic crust increases, the wave train of the Lg is lengthened drastically.

For all the cases of the presence of the basin, either with a Moho-uplift or without a Moho-uplift, and when the locations of observation are beyond the left limb of the basin, there are several wave-packet-like arrivals observed. The ones followed S_n may be interpreted as the conversion of the S_n -to-Lg wave from the interface.

Another interesting feature is that there show minimum S_n arrivals in the adjacent of the left limb of the basin.

The amplitude variations of the seismic responses for the cases with Moho-uplift, in comparison with the corresponding cases with no Moho-uplift, depend on the observation locations and the frequency contents. To understand the mechanism of Lg propagation, further systematic investigation is needed.

FUTURE WORKS

The first year investigation of the problem of the blockage of the Lg waves due to the island margin to the Barents Sea has laid the foundation for the future work.

In order to understand the problem of the blockage of the Lg wave propagation in a laterally inhomogeneous earth, systematic studies must be continued, including the following:

(1) Replace the the averaged granitic/basaltic crust by a crust consisted of two separate layers with different geophysical parameters. (2) The problem of the sensitivities of various geometrical and material parameters, viz., (i) the size of the basin e.g., the ratio of the depth to the width of the basin; (ii) the dip angle of the basin sides; (iii) the variation of thickness of the crust, (iv) the crustal-Q variations, to the variations of Lg amplitude. (3) Extend the present study to the problem for the cases of elastodynamics i.e. P and S waves.

Moreover, we shall extend the Island Margin, the Basin, and the Basin and Crust Pinch models to include the Baltic Shield and European Continent to ARESS, NORESS and Graefenburg. If time permits, we shall compare the FEM results with the observations.

CONCLUSIONS

During the first year of the Contract F49620-93-1-0073, we have studied the problem of the blockage of Lg waves by the finite element models of island Margin, basin, and basin with an uplifted Moho to simulate the great-circle path from Novaya Zemlya to the Barnets Sea.

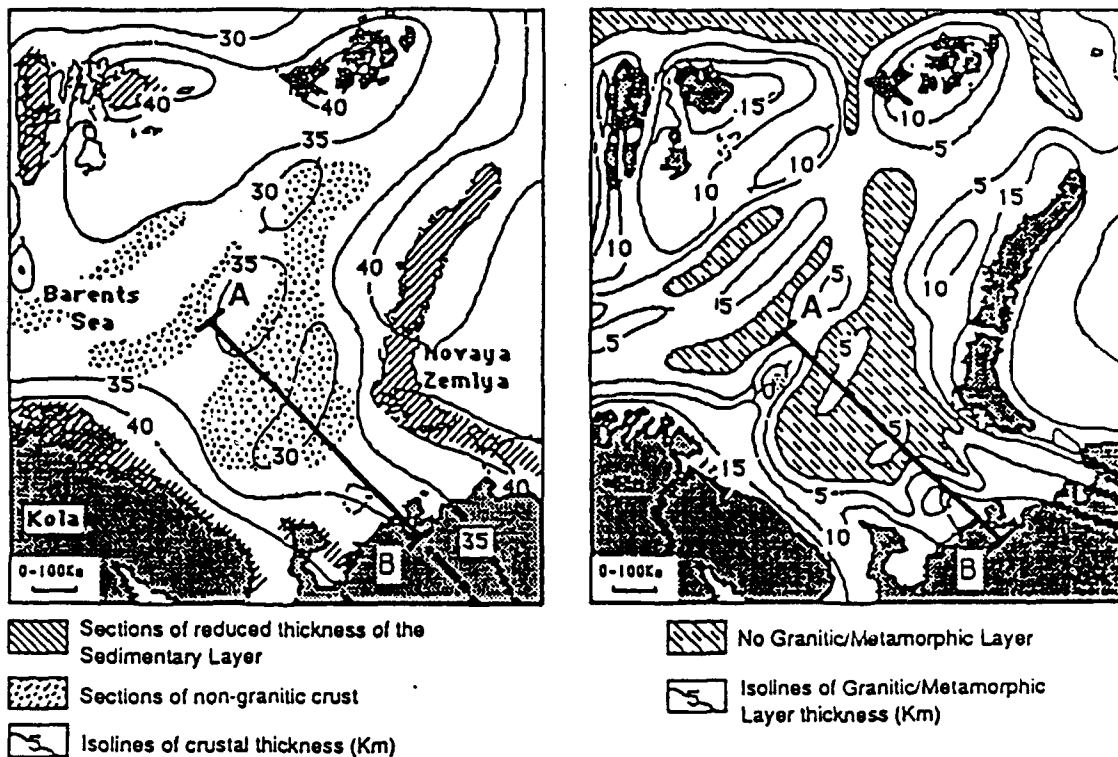
The efficiency of the crust (an averaged granitic/basaltic crust in the present case) as a wave guide of the Lg waves strongly depend on the frequency content of an impulsive source.

The effects of the presence of a basin in the crust on the Lg wave propagation depend on frequency content of the source, the width of the basin and the velocity contrast between the sedimentary basin and the surrounding crust.

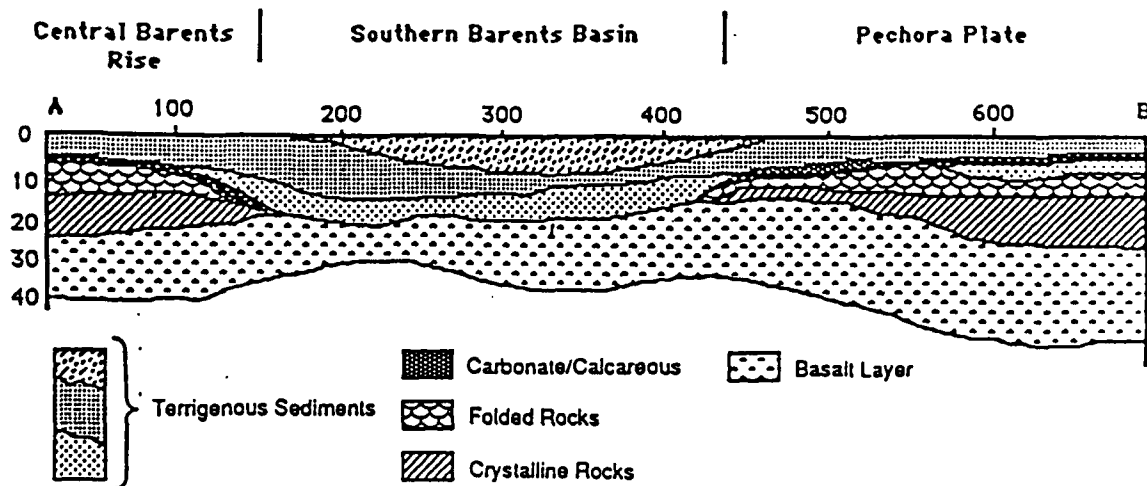
The presence of an uplifted Moho alone appears to have a minor blockage effect on the Lg wave propagation.

In order to understand the blockage and characteristics of Lg waves, it is insufficient to investigate the Lg waves on the earth surface alone. It is fruitful to study the evolutionary characteristics of Lg waves in the interior of the crust and the upper mantle.

The finite element codes with the fast execution algorithm proves to be a well suited tool for the modeling purpose intended in this research.



(a)



(b)

FIGURE 1 (A) GEOLOGIC MAPS OF BARENTS SEA BASIN (AFTER GRAMBERG, 1988). (B) NW-SE CROSS SECTION (AB) ACROSS THE BASIN. (After Baumgardt, 1990b)

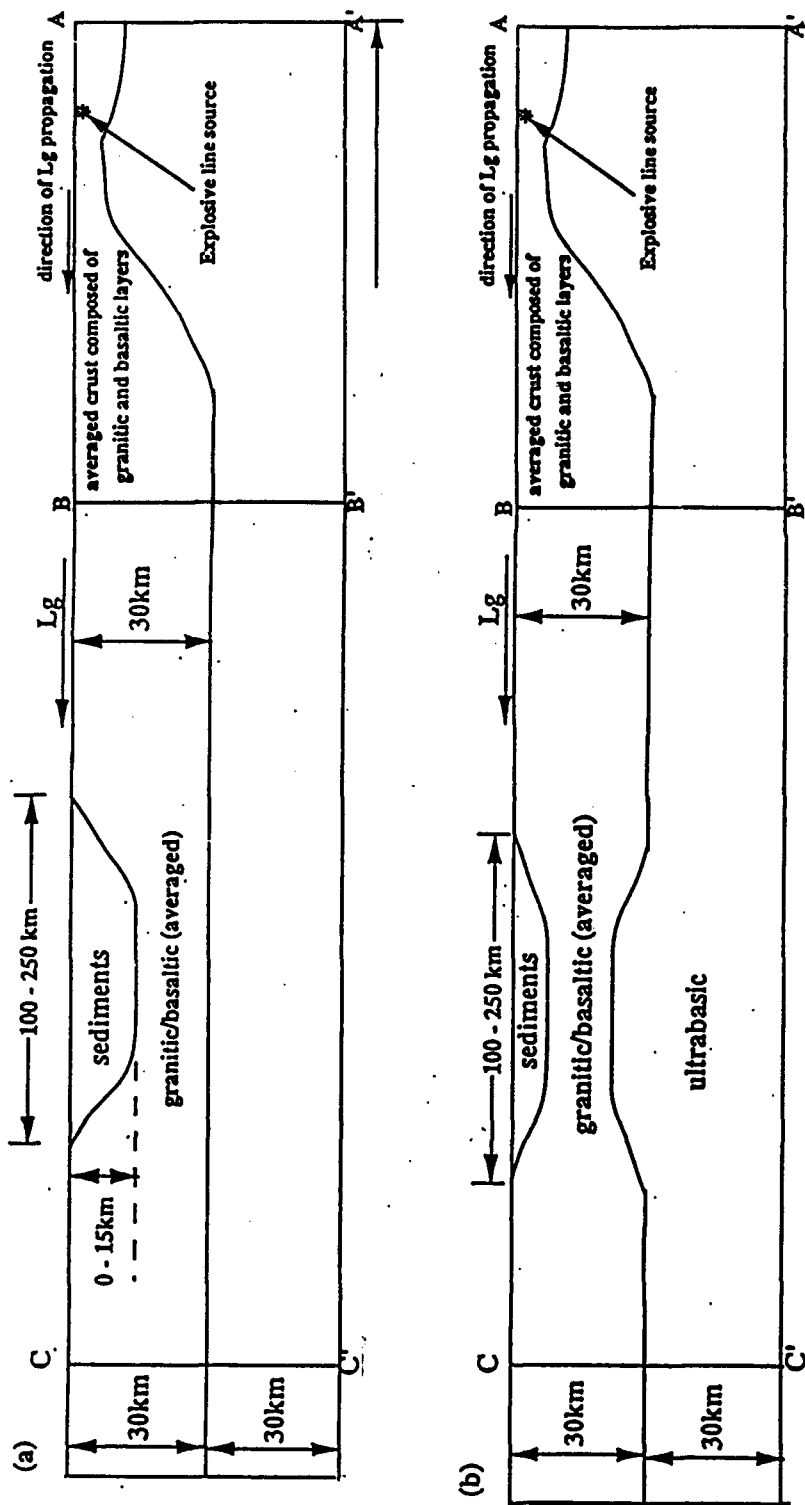


Figure 2. (a) Model I simulating the geological structure along the path from the former USSR nuclear test sites Novaya Zemlya to the Barents Sea, which is represented by a sedimentary basin. (b) Model II simulating the geological structure along the path from the former USSR nuclear test sites Novaya Zemlya to the Barents Sea, which is represented by a sedimentary basin as in Figure 2-(a); in addition, the Moho is assumed to have been uplifted with an identical anti-dip of the sedimentary basin.

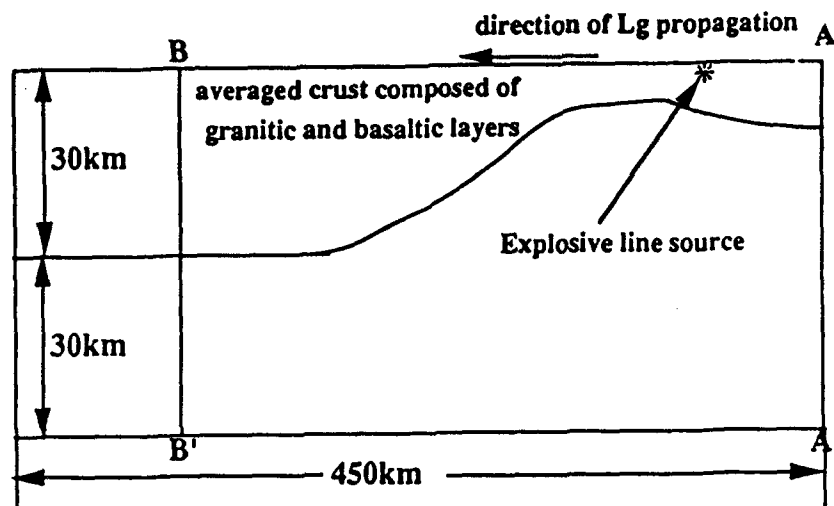


Figure 3-(a) The Island Margin Model

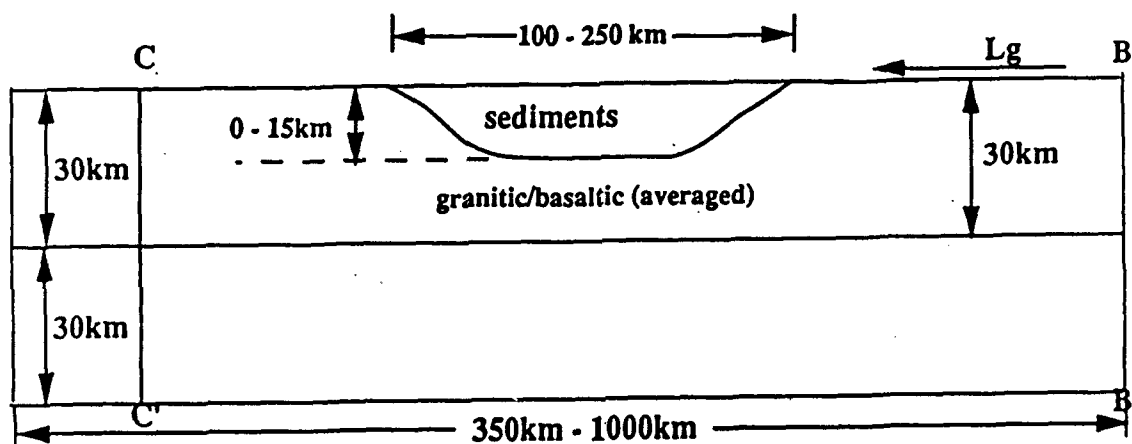


Figure 3-(b) The Basin Model

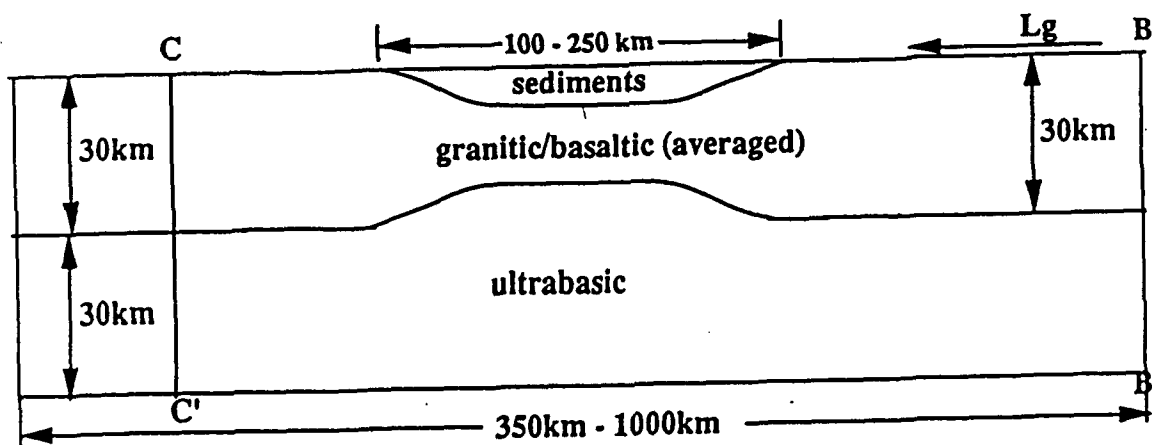


Figure 3-(c) The Basin and Crust-Pinch Model

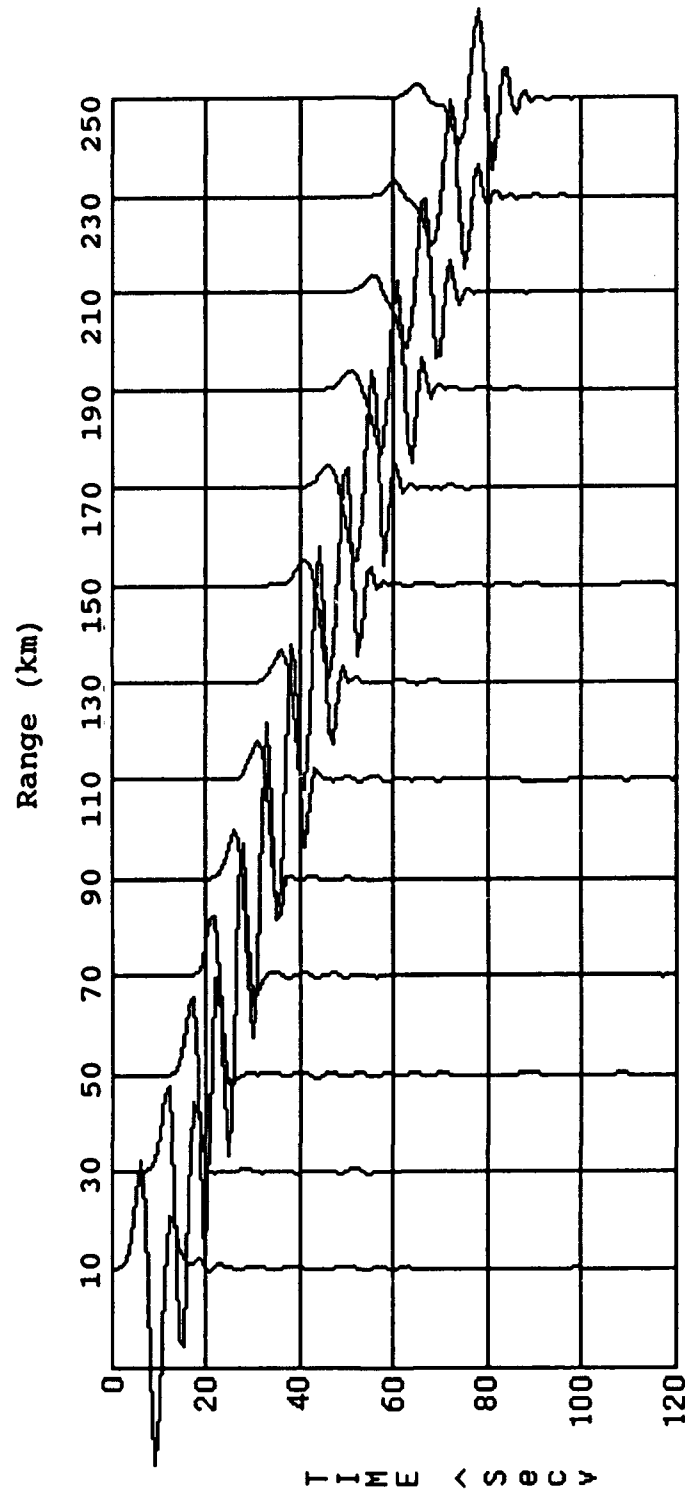


Figure 4-(a). The finite-element synthetic seismogram of Lg waves by an impulsive line source with center frequency of 0.167 Hz as observed at distances of 10 km to 250 km from the source of the Island Margin Model A.

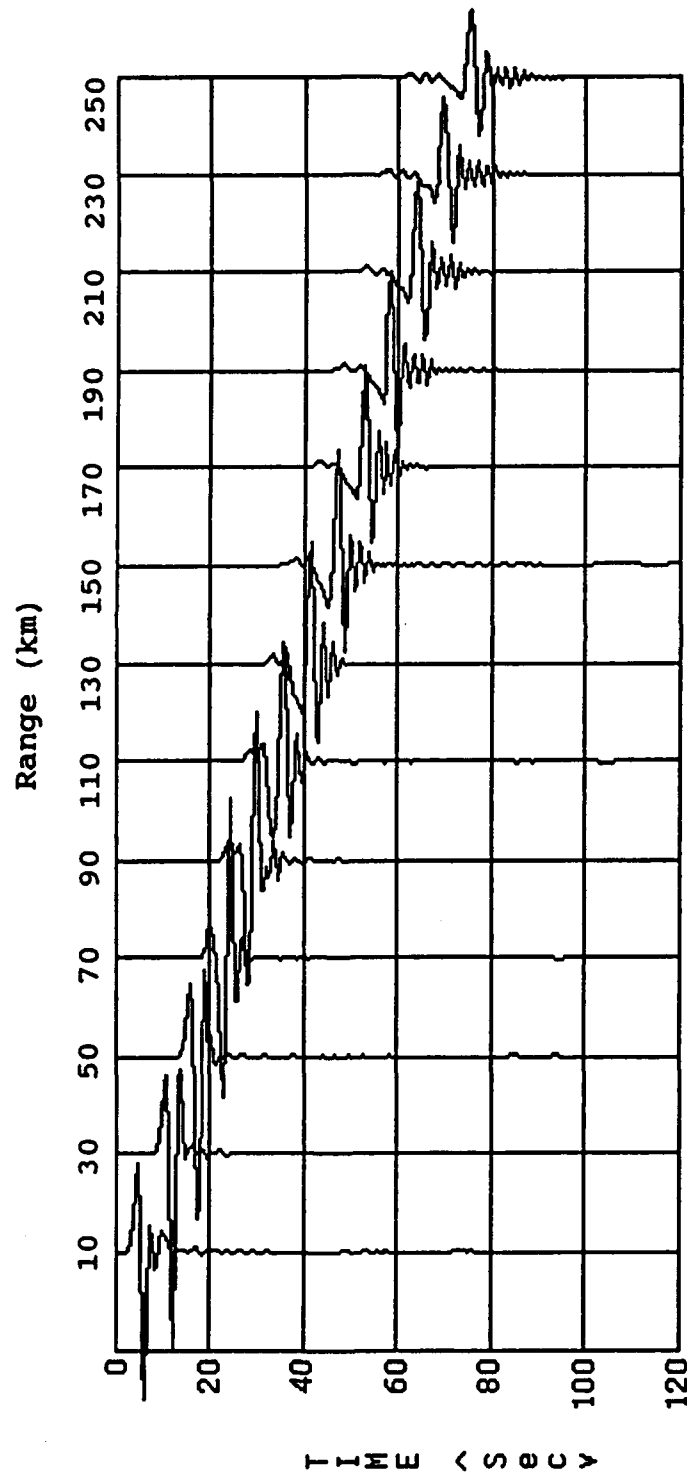


Figure 4-(b). The finite-element synthetic seismogram of Lg waves by an impulsive line source with center frequency of 0.334 Hz as observed at distances of 10 km to 250 km from the source of the Island Margin Model A.

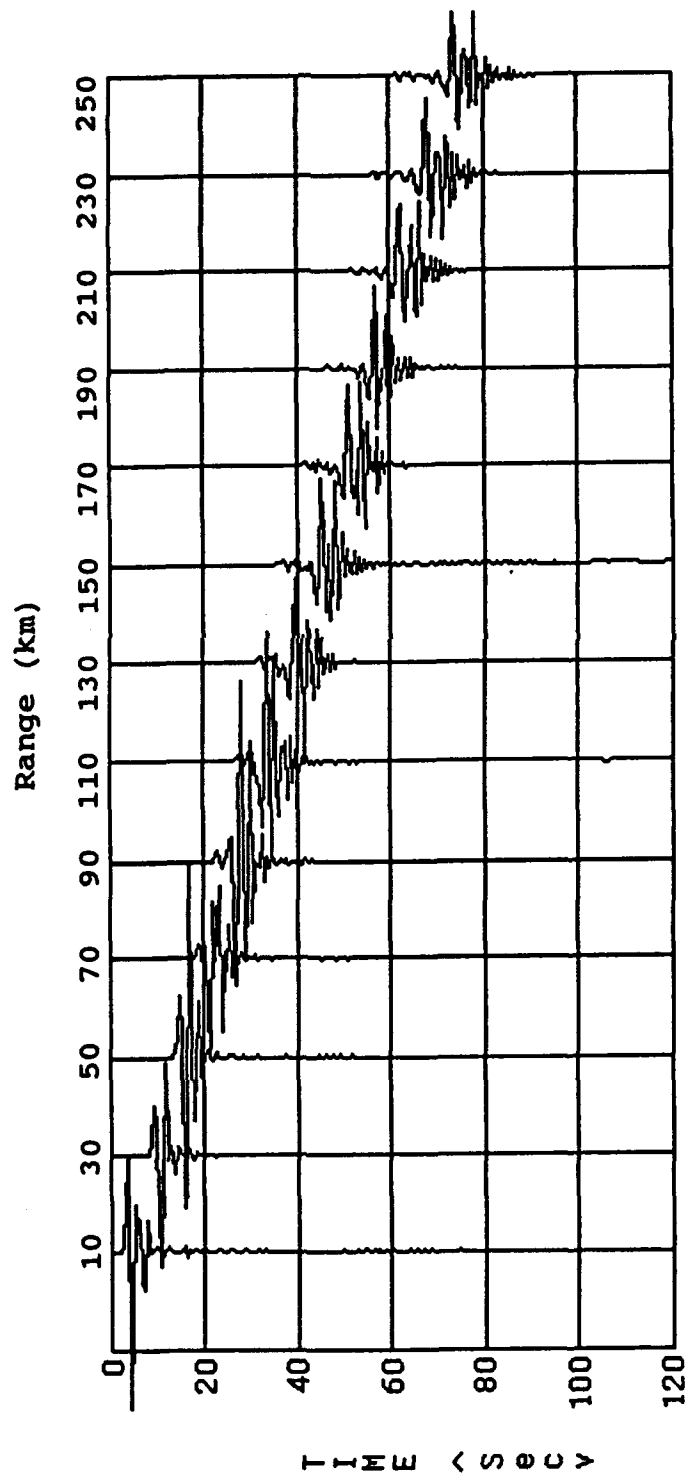


Figure 4-(c). The finite-element synthetic seismogram of Lg waves by an impulsive line source with center frequency of 0.667 Hz as observed at distances of 10 km to 250 km from the source of the Island Margin Model A.

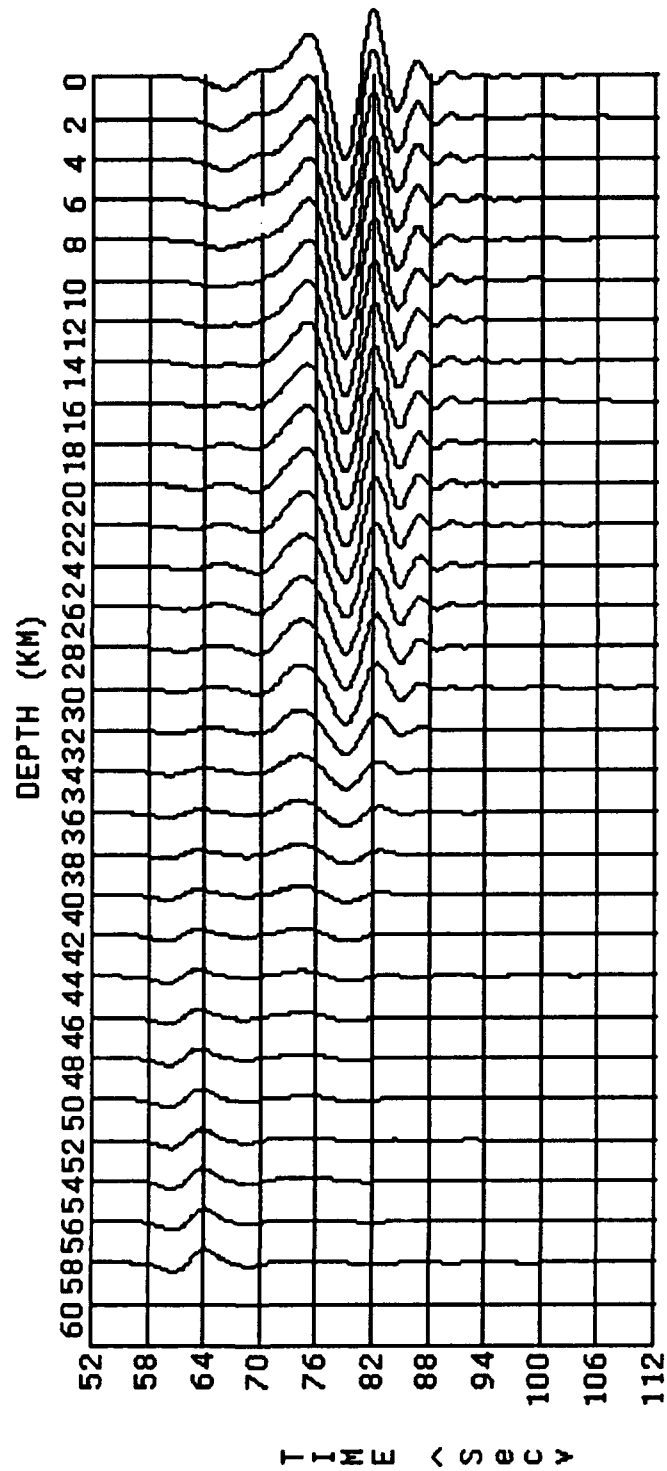


Figure 5-(a). The seismic responses of Lg waves by an impulsive source with center frequency of 0.167 Hz as observed along the vertical section BB' of the Island Margin Margin Model A, which are used to exite the Basin Model B.

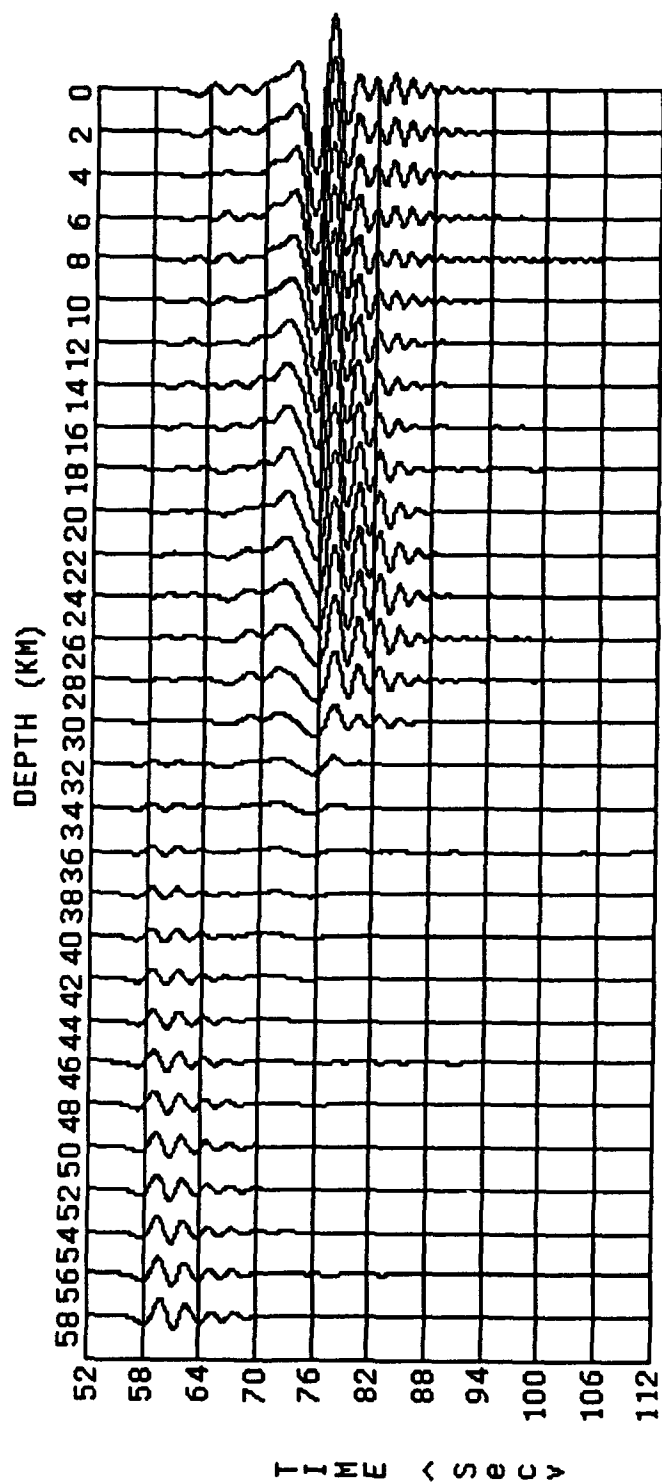


Figure 5-(b). The seismic responses of Lg waves by an impulsive source with center frequency of 0.334 Hz as observed along the vertical section BB' of the Island Margin Margin Model A, which are used to exite the Basin Model B.

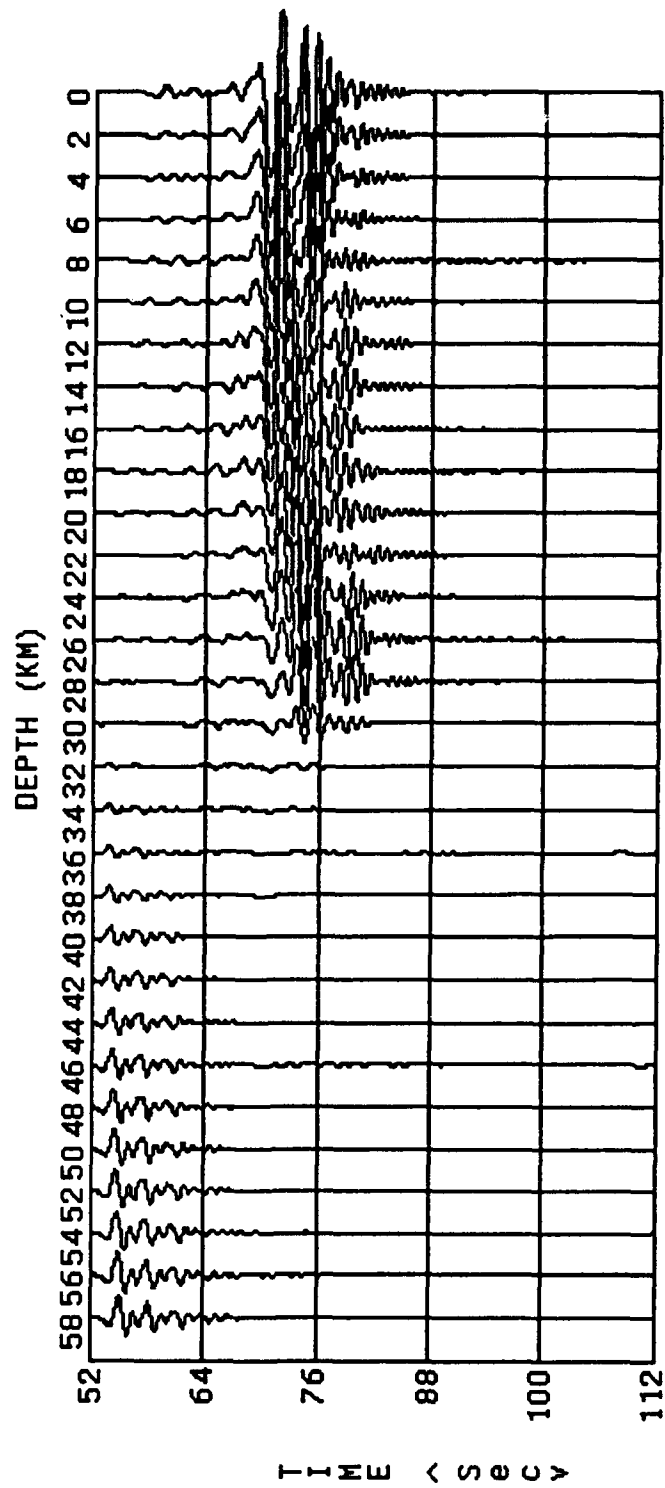


Figure 5-(c). The seismic responses of Lg waves by an impulsive source with center frequency of 0.667 Hz as observed along the vertical section BB' of the Island Margin Margin Model A, which are used to exite the Basin Model B.

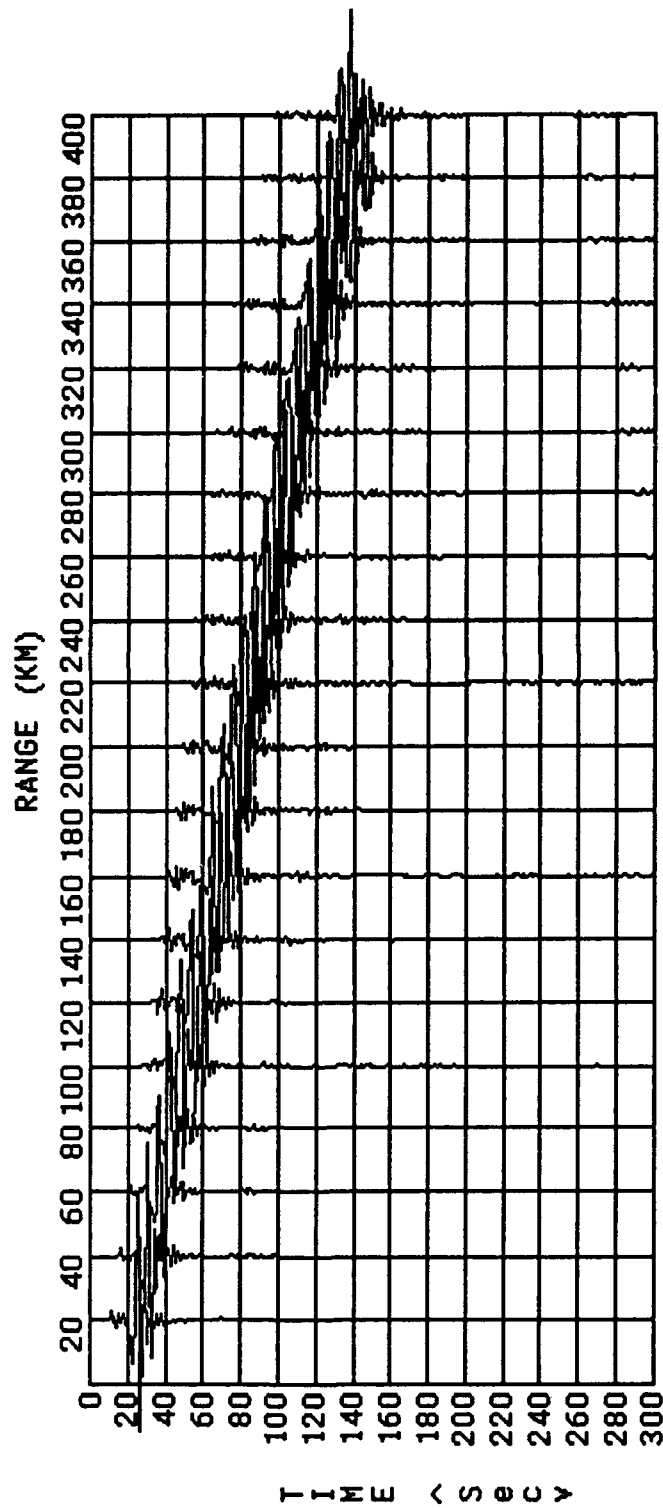


Figure 6-(a). The finite-element synthetic seismogram for the Basin Model of Figure 3-(b), (basin width = 150 km, basin depth = 15 km), with the basin velocity of 3.51 km/sec, as observed at distances of 20 km to 400 km by a source with a center frequency 0.334 Hz. (the basin is replaced by averaged granitic/basaltic material, i.e. no basin.)

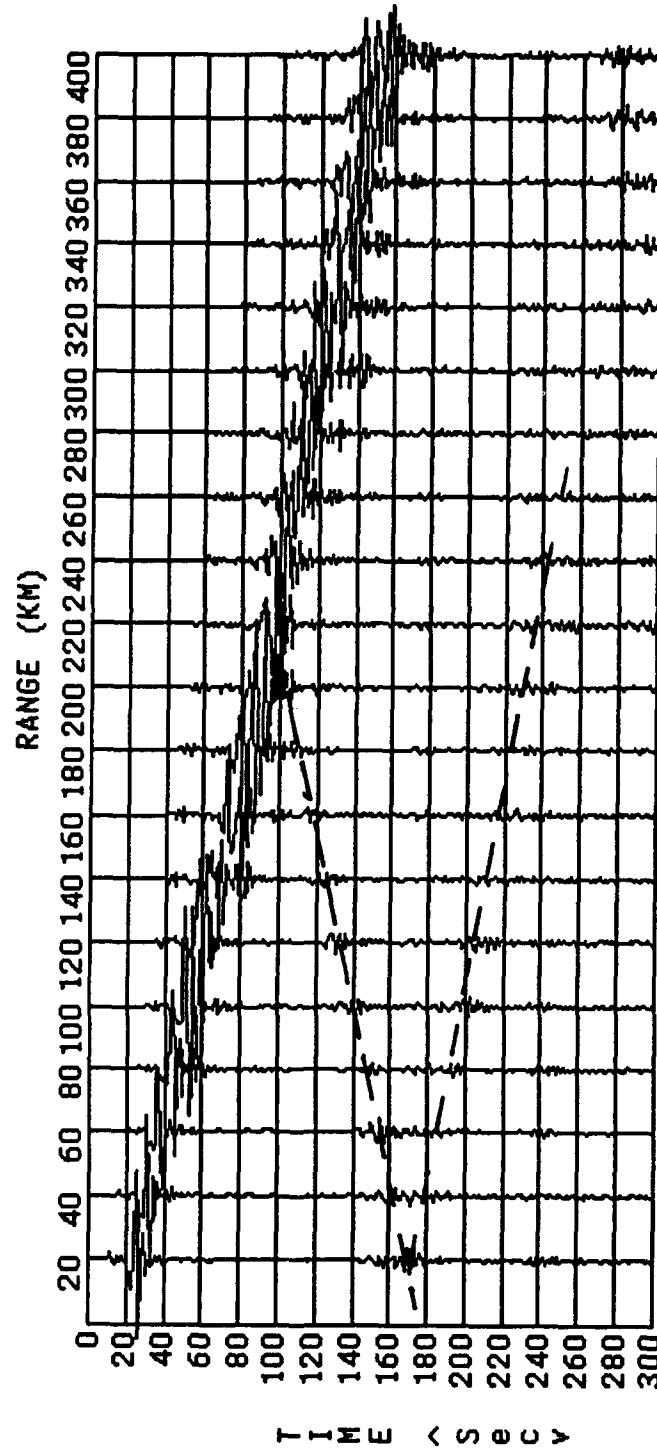


Figure 6-(b). The finite-element synthetic seismogram for the Basin Model of Figure 3-(b), (basin width = 150 km, basin depth = 15 km), with the basin velocity of 2.70 km/sec, as observed at distances of 20 km to 400 km by a source with a center frequency 0.334 Hz. (the basin is replaced by averaged granitic/basaltic material, i.e. no basin.)

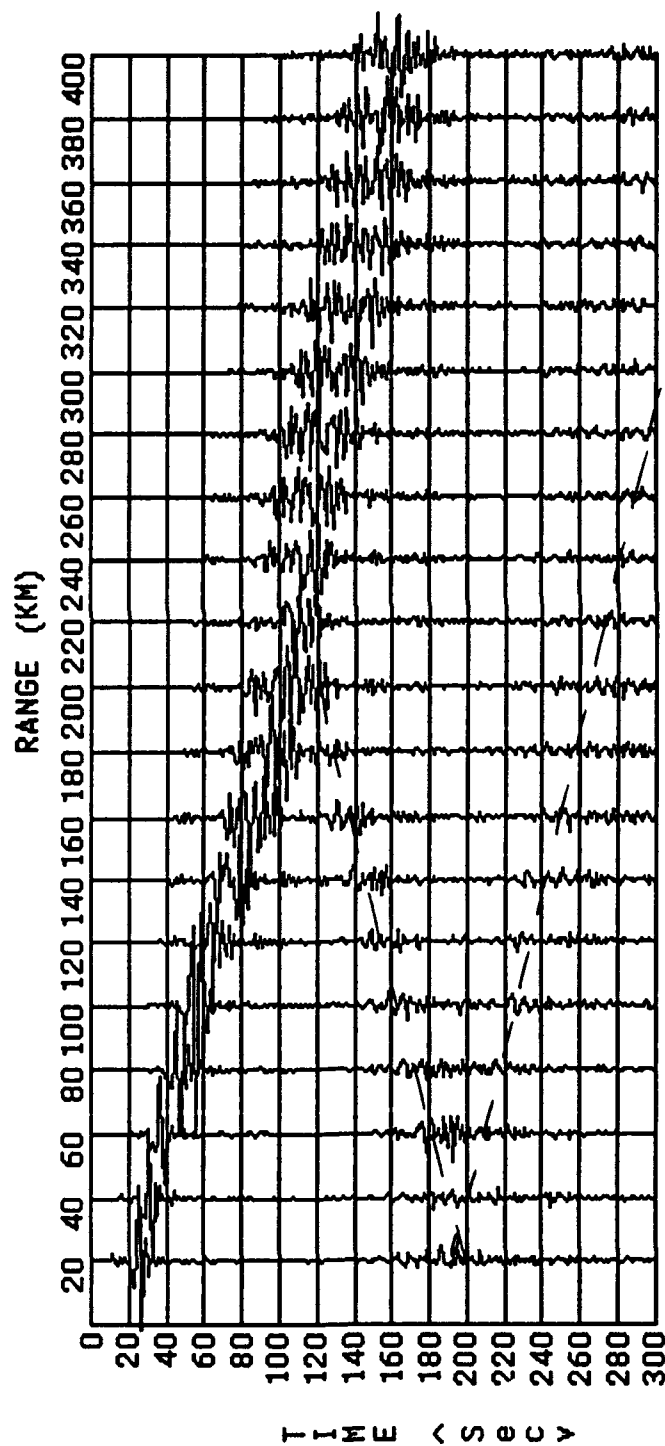


Figure 6-(c). The finite-element synthetic seismogram for the Basin Model of Figure 3-(b), (basin width = 150 km, basin depth = 15 km), with the basin velocity of 2.20 km/sec, as observed at distances of 20 km to 400 km by a source with a center frequency 0.334 Hz. (the basin is replaced by averaged granitic/basaltic material, i.e. no basin.)

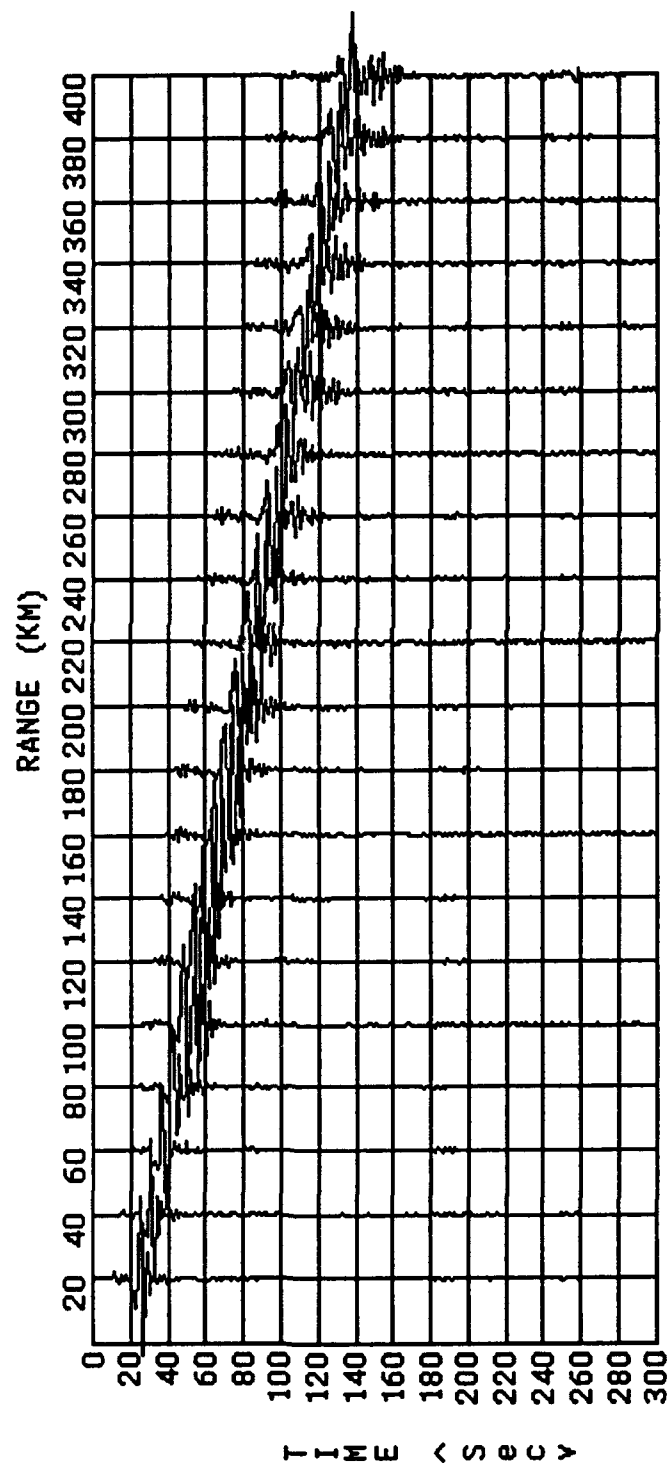


Figure 6-(d). The finite-element synthetic seismogram for the Basin and Crust-Pinch Model of Figure 3-(c), (basin width = 150 km, basin depth = 15 km, height of Moho-uplift = 10 km), with the basin velocity of 3.51 km/sec, as observed at distances of 20 km to 400 km by a source with a center frequency 0.334 Hz (no basin).

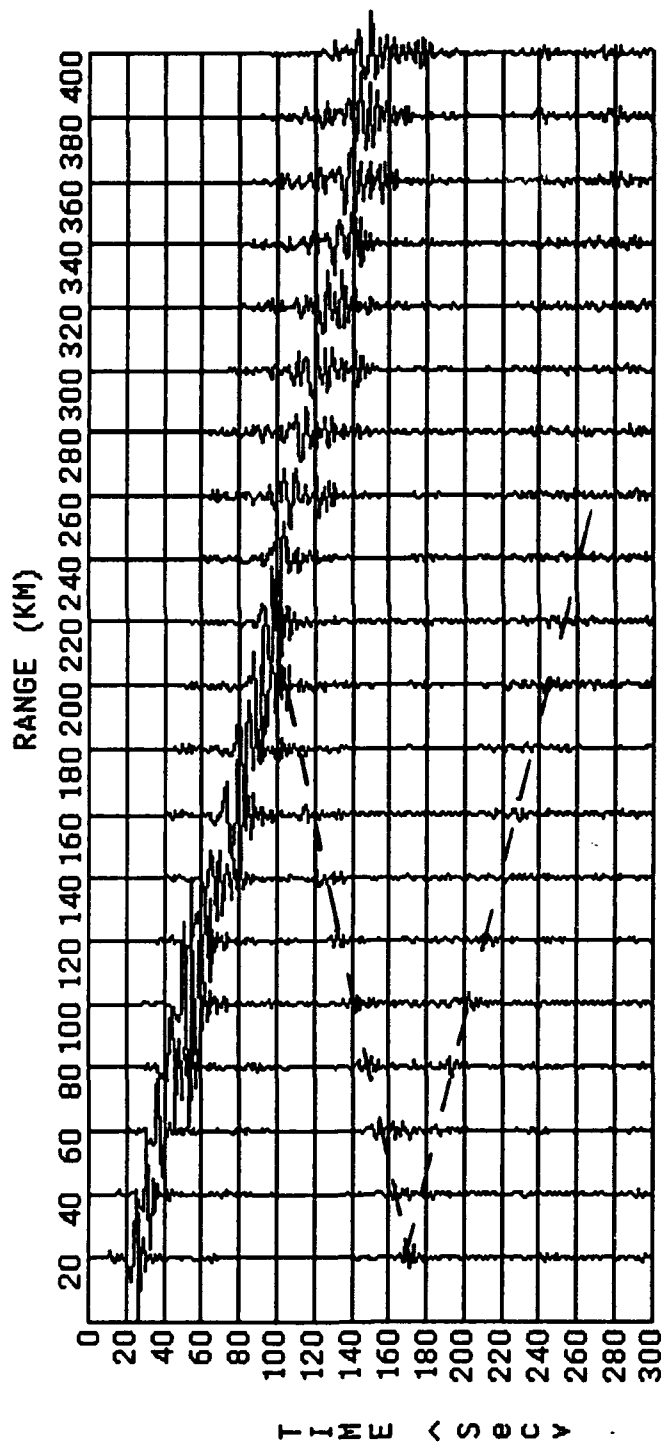


Figure 6-(e). The finite-element synthetic seismogram for the Basin and Crust-Pinch Model of Figure 3-(c), (basin width = 150 km, basin depth = 15 km, height of Moho-uplift = 10 km), with the basin velocity of 2.70 km/sec, as observed at distances of 20 km to 400 km by a source with a center frequency 0.334 Hz.

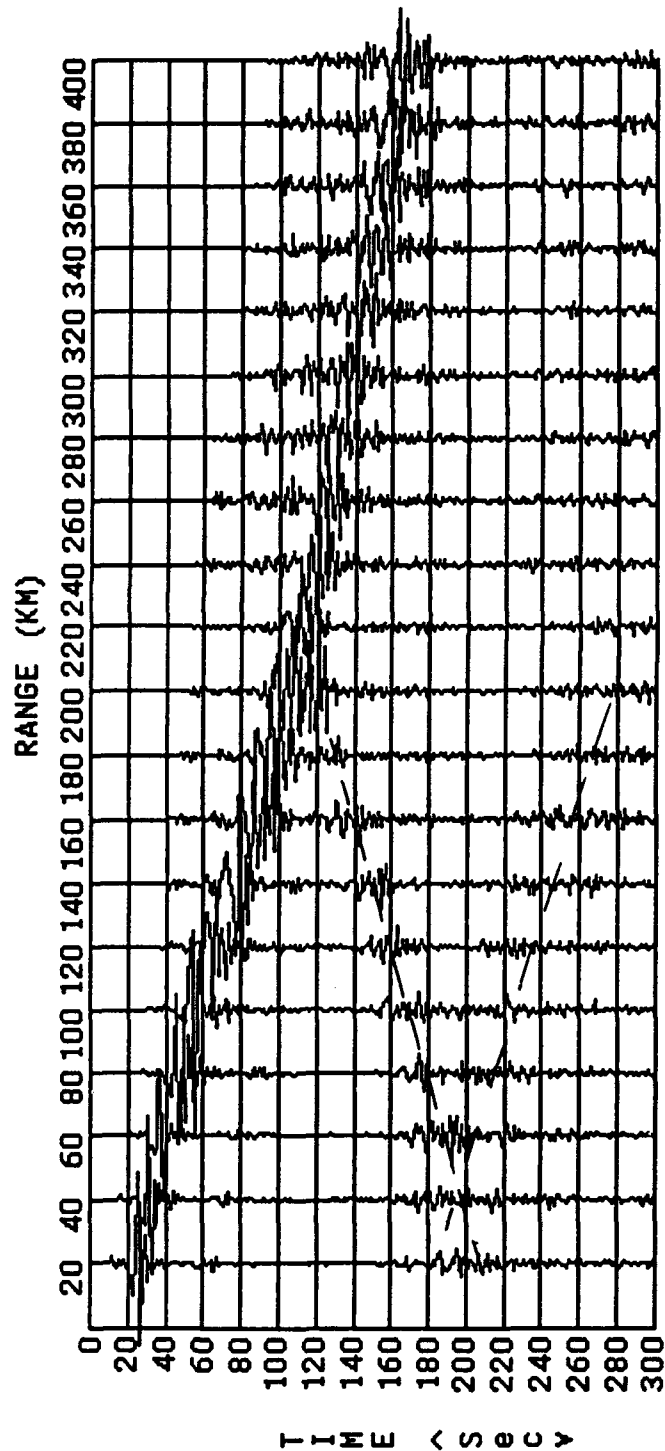


Figure 6-(f). The finite-element synthetic seismogram for the Basin and Crust-Pinch Model of Figure 3-(c), (basin width = 150 km, basin depth = 15 km, height of Moho-uplift = 10 km), with the basin velocity of 2.20 km/sec, as observed at distances of 20 km to 400 km by a source with a center frequency 0.334 Hz.

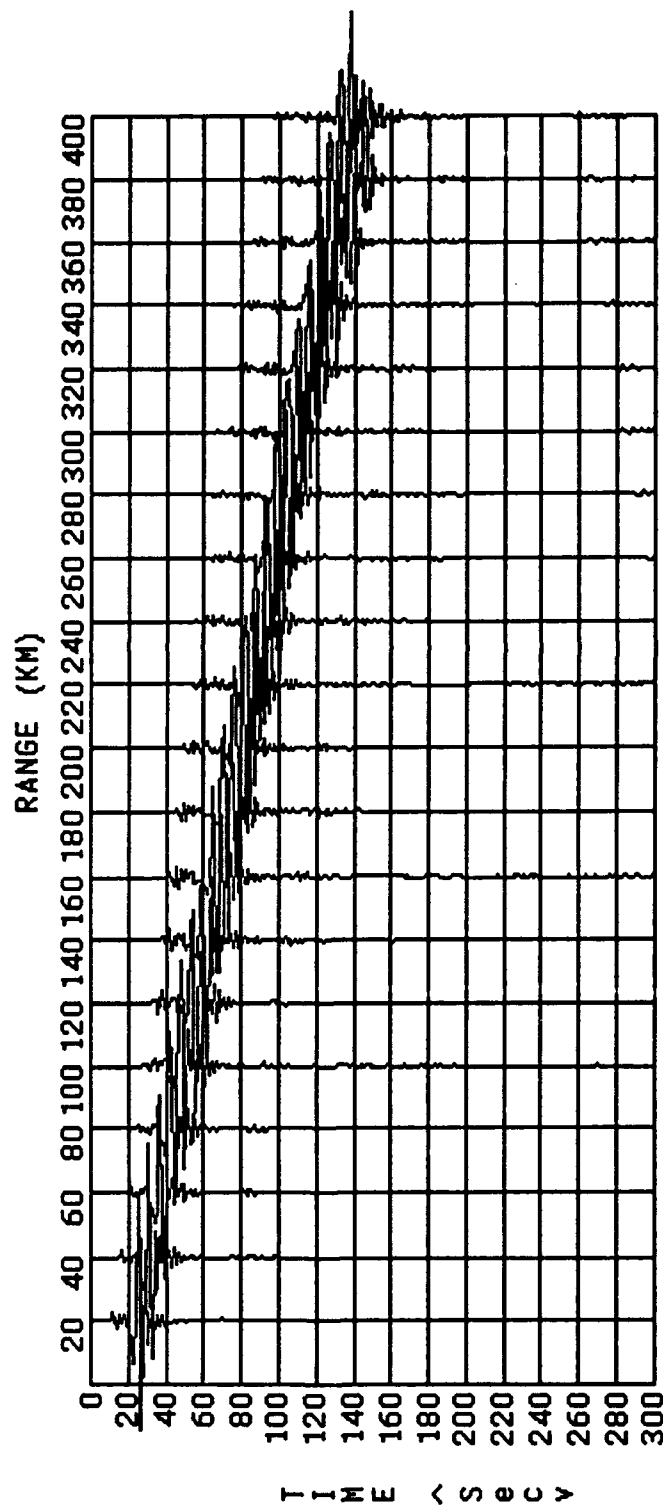


Figure 7-(a). The finite-element synthetic seismogram for the Basin Model of Figure 3-(b), (basin width = 250 km, basin depth = 15 km), with the basin velocity of 3.51 km/sec, as observed at distances of 20 km to 400 km by a source with a center frequency 0.334 Hz. (virtually identical to Figure 6-(a).)

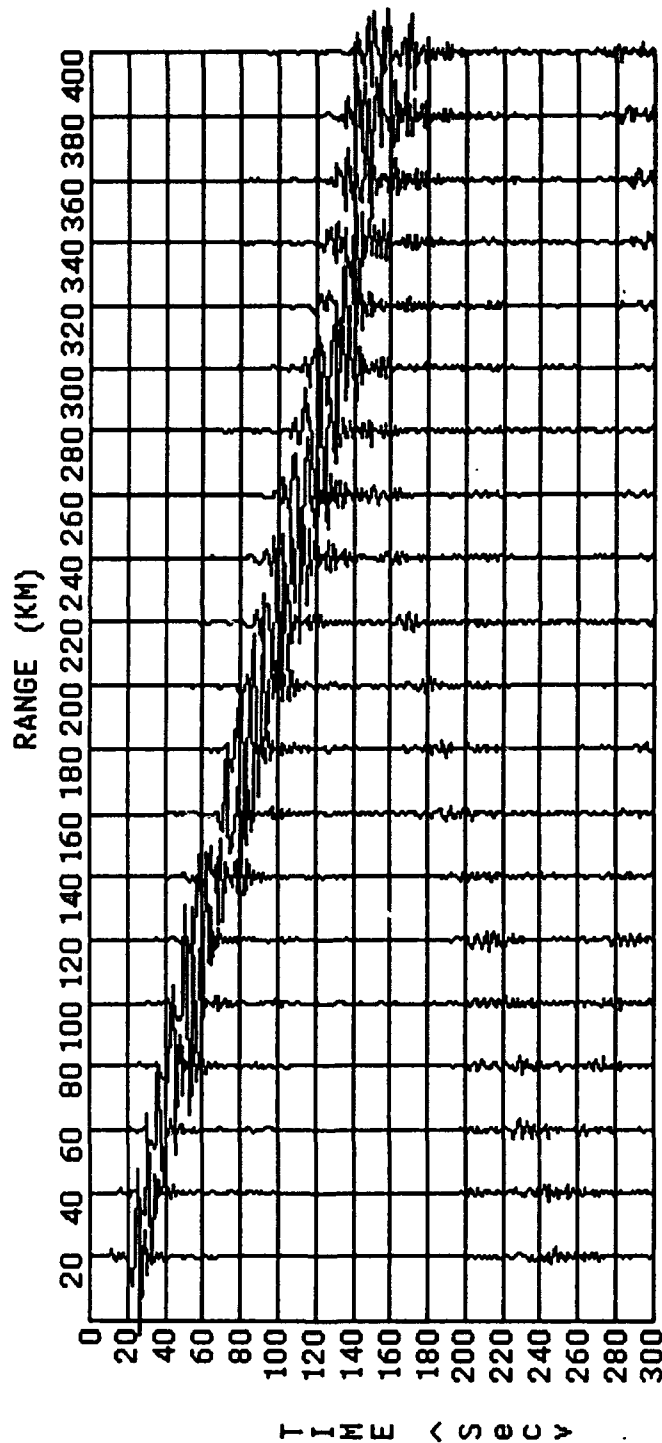


Figure 7-(b). The finite-element synthetic seismogram for the Basin Model of Figure 3-(b), (basin width = 250 km, basin depth = 15 km), with the basin velocity of 2.70 km/sec, as observed at distances of 20 km to 400 km by a source with a center frequency 0.334 Hz. (the basin is replaced by averaged granitic/basaltic material, i.e. no basin.)

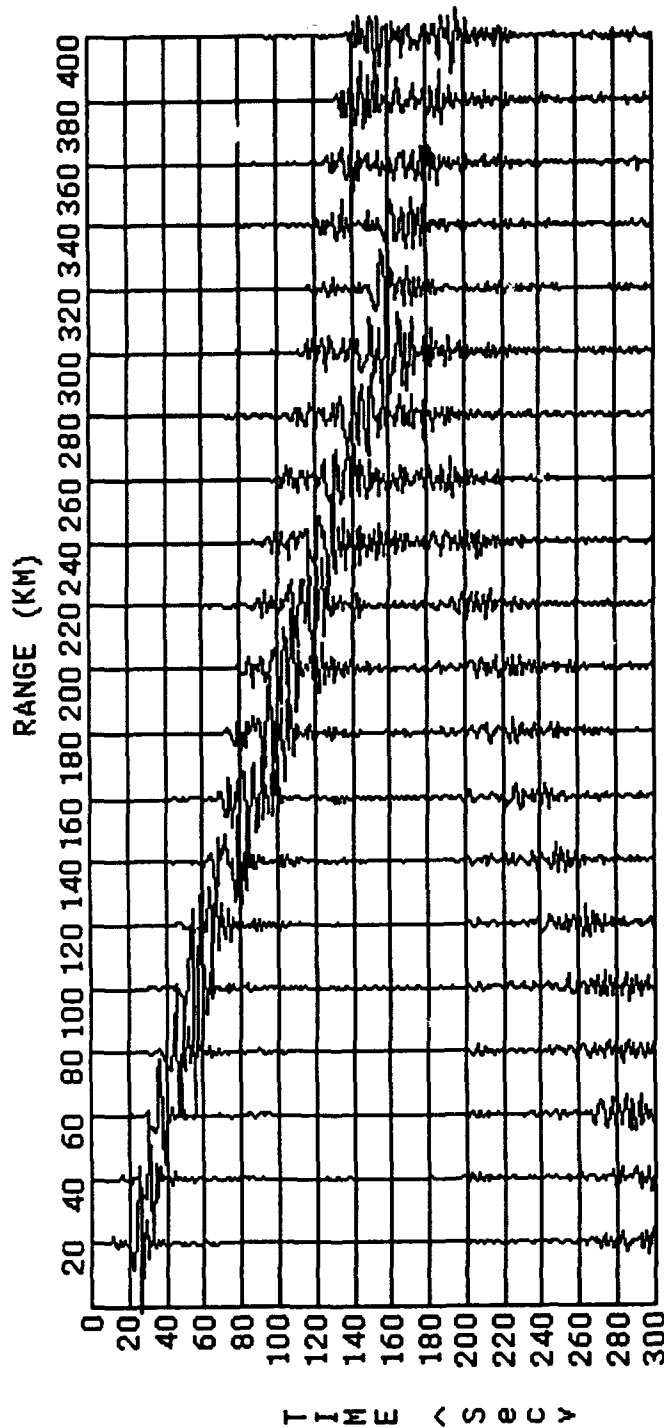


Figure 7-(c). The finite-element synthetic seismogram for the Basin Model of Figure 3-(b), (basin width = 250 km, basin depth = 15 km), with the basin velocity of 2.20 km/sec, as observed at distances of 20 km to 400 km by a source with a center frequency 0.334 Hz. (the basin is replaced by averaged granitic/basaltic material, i.e. no basin.)

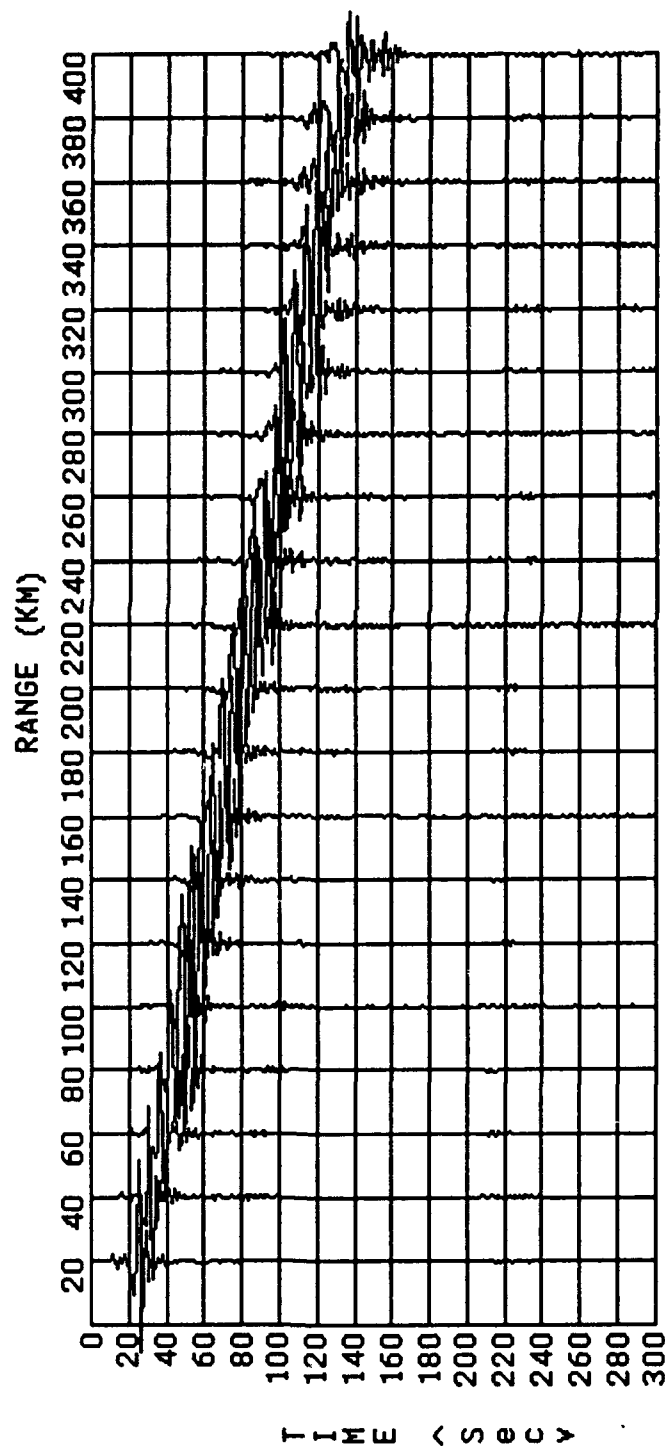


Figure 7-(d). The finite-element synthetic seismogram for the Basin and Crust-Pinch Model of Figure 3-(c), (basin width = 250 km, basin depth = 15 km, height of Moho-uplift = 10 km), with the basin velocity of 3.51 km/sec, as observed at distances of 20 km to 400 km by a source with a center frequency 0.334 Hz (no basin).

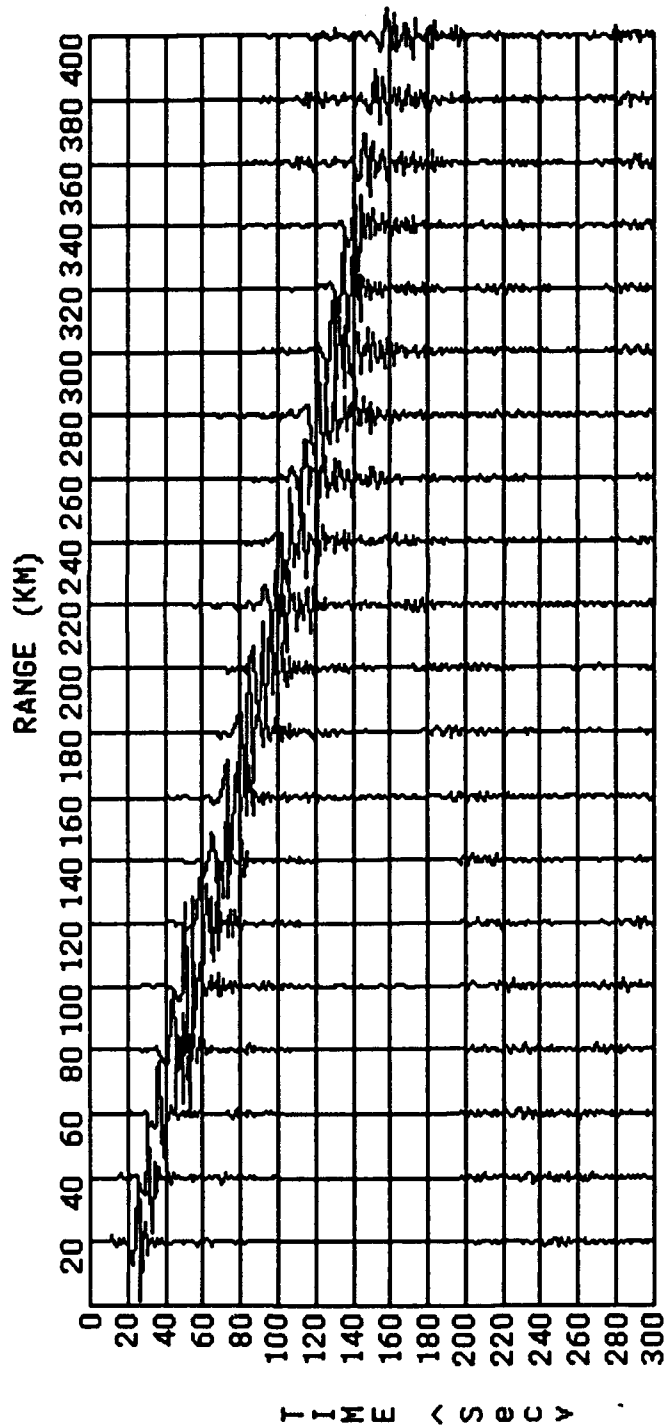


Figure 7-(e). The finite-element synthetic seismogram for the Basin and Crust-Pinch Model of Figure 3-(c), (basin width = 250 km, basin depth = 15 km, height of Moho-uplift = 10 km), with the basin velocity of 2.70 km/sec, as observed at distances of 20 km to 400 km by a source with a center frequency 0.334 Hz.

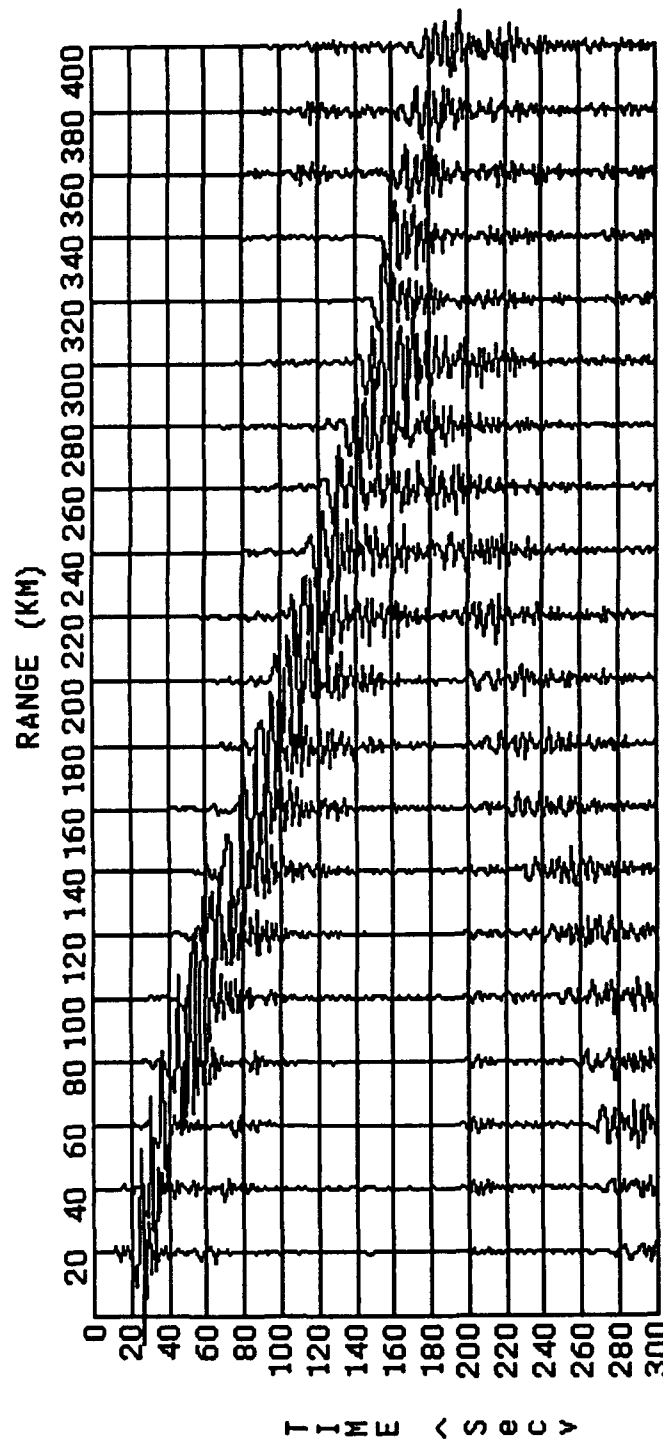


Figure 7-(f). The finite-element synthetic seismogram for the Basin and Crust-Pinch Model of Figure 3-(c), (basin width = 250 km, basin depth = 15 km, height of Moho-uplift = 10 km), with the basin velocity of 2.20 km/sec, as observed at distances of 20 km to 400 km by a source with a center frequency 0.334 Hz.

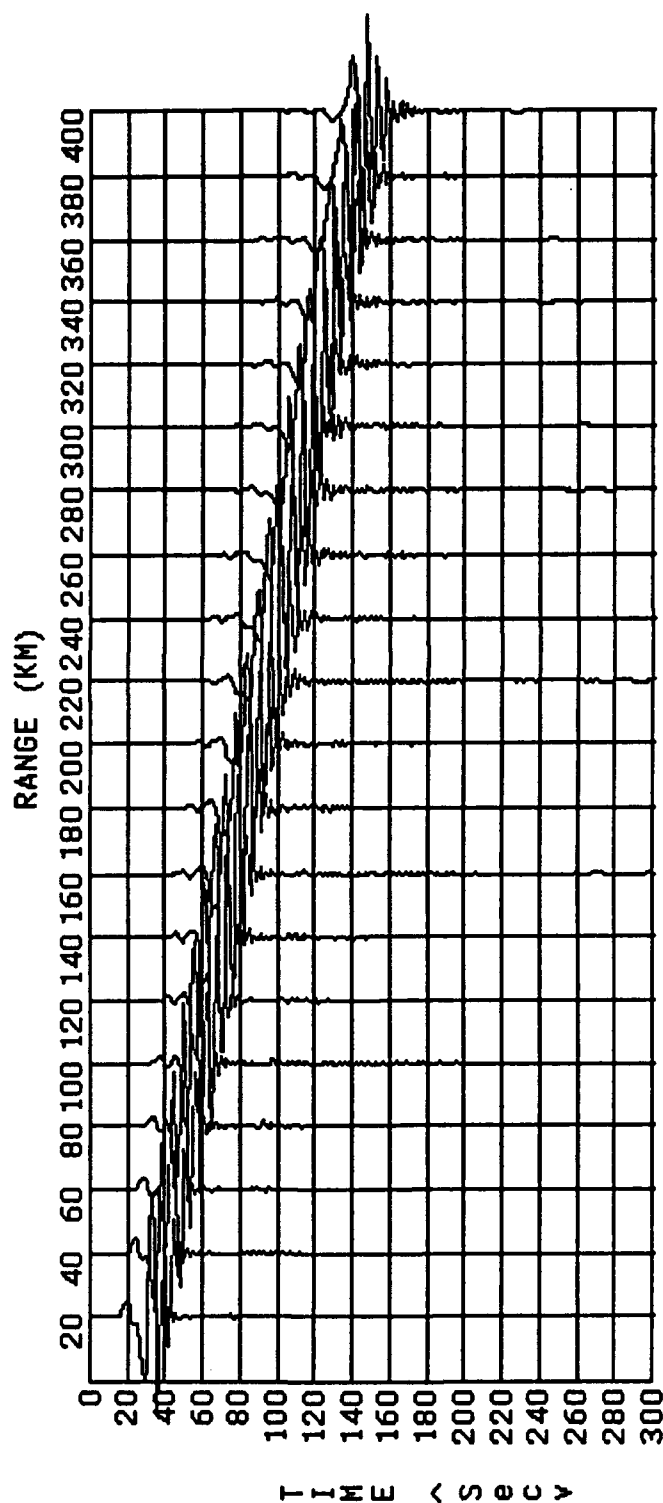


Figure 8-(a). The finite-element synthetic seismogram for the Basin Model of Figure 3-(b), (basin width = 250 km, basin depth = 15 km), with the basin velocity of 3.51 km/sec, as observed at distances of 20 km to 400 km by a source with a center frequency 0.167 Hz. (the basin is replaced by averaged granitic/basaltic material, i.e. no basin.)

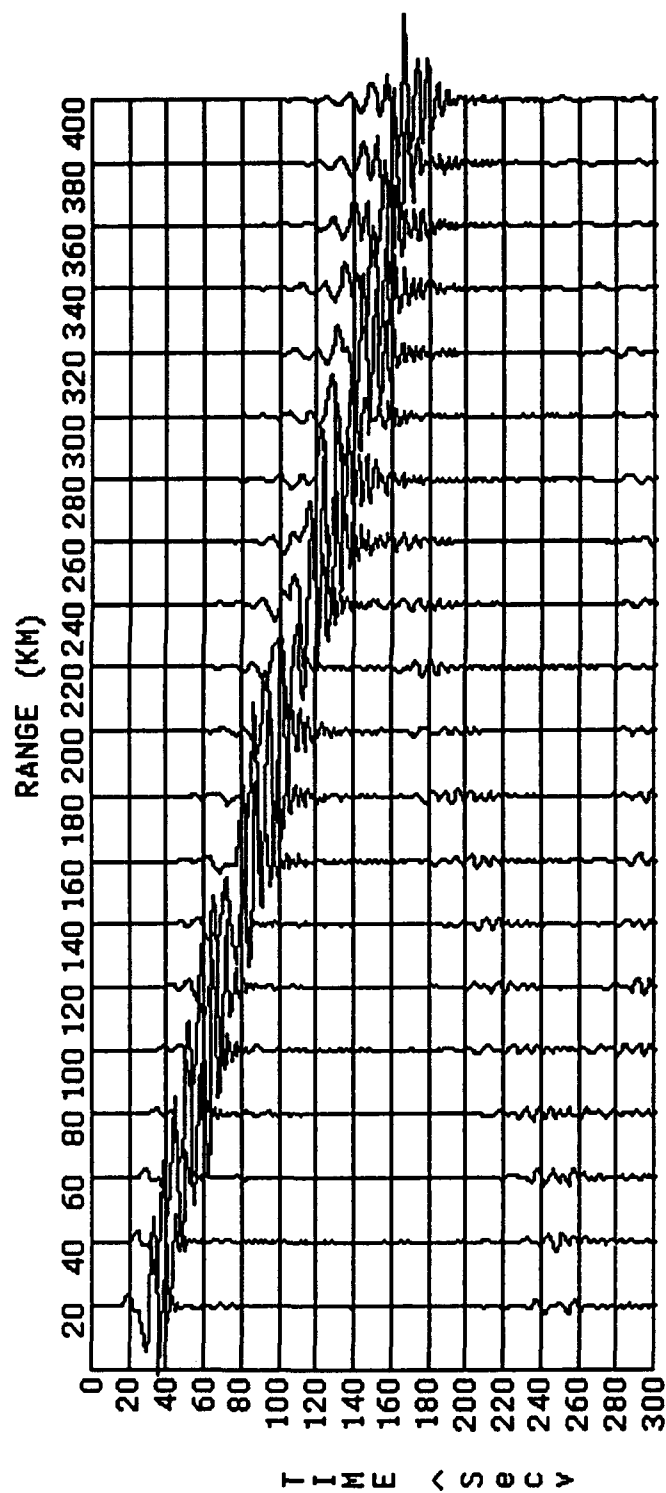


Figure 8-(b). The finite-element synthetic seismogram for the Basin Model of Figure 3-(b), (basin width = 250 km, basin depth = 15 km), with the basin velocity of 2.70 km/sec, as observed at distances of 20 km to 400 km by a source with a center frequency 0.167 Hz. (the basin is replaced by averaged granitic/basaltic material, i.e. no basin.)

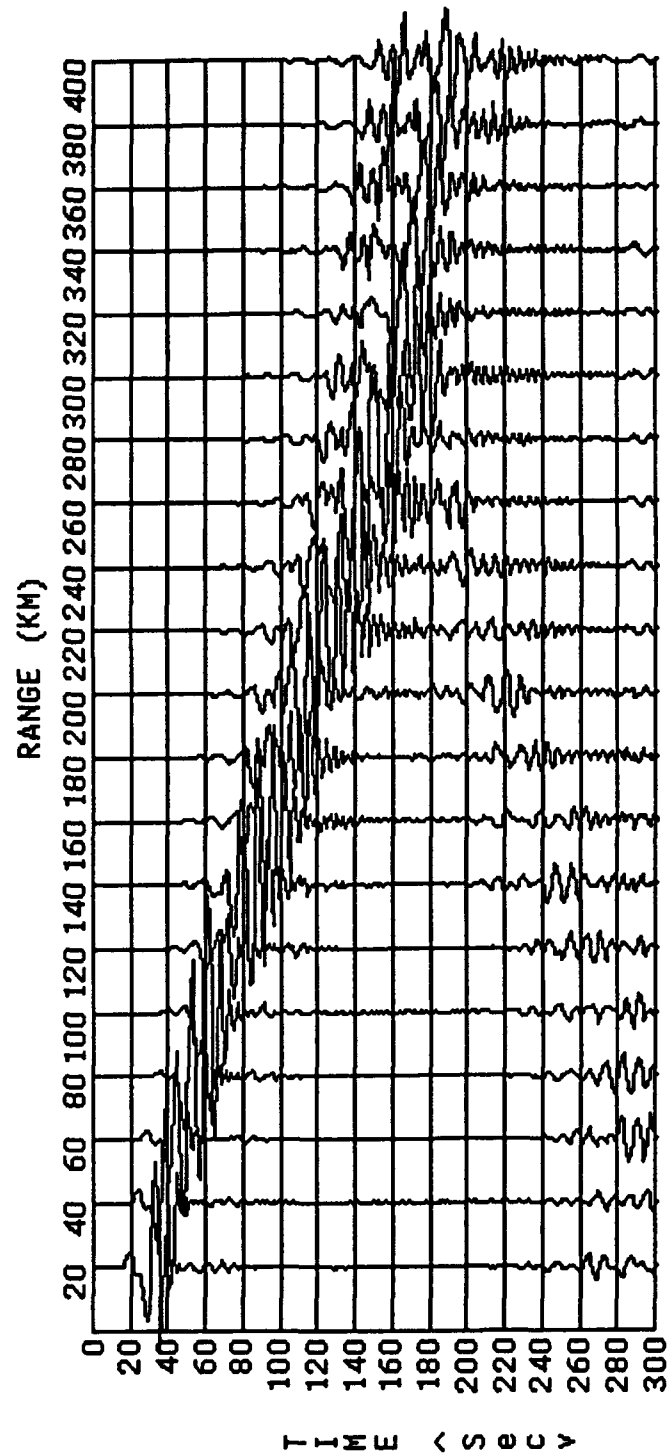


Figure 8-(c). The finite-element synthetic seismogram for the Basin Model of Figure 3-(b), (basin width = 250 km, basin depth = 15 km), with the basin velocity of 2.20 km/sec, as observed at distances of 20 km to 400 km by a source with a center frequency 0.167 Hz. (the basin is replaced by averaged granitic/basaltic material, i.e. no basin.)

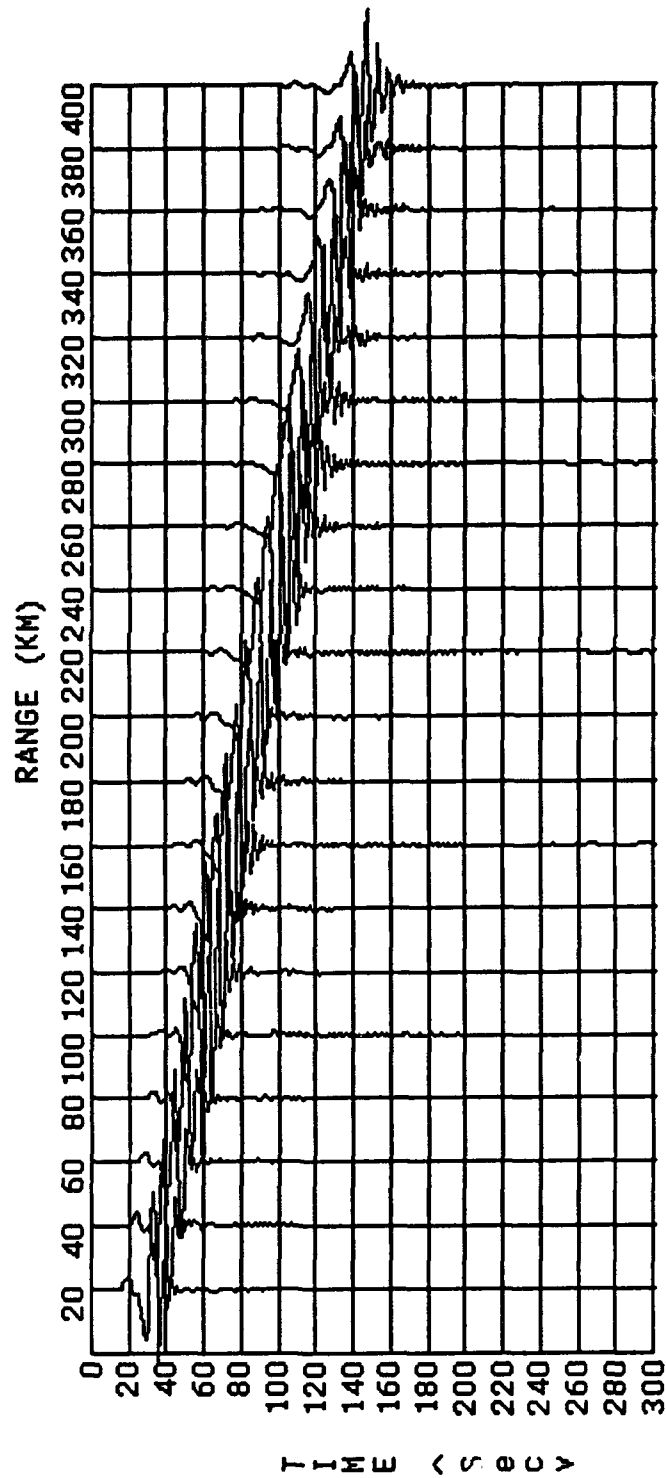


Figure 8-(d). The finite-element synthetic seismogram for the Basin and Crust-Pinch Model of Figure 3-(c), (basin width = 250 km, basin depth = 15 km, height of Moho-uplift = 10 km), with the basin velocity of 3.51 km/sec, as observed at distances of 20 km to 400 km by a source with a center frequency 0.167 Hz (no basin).

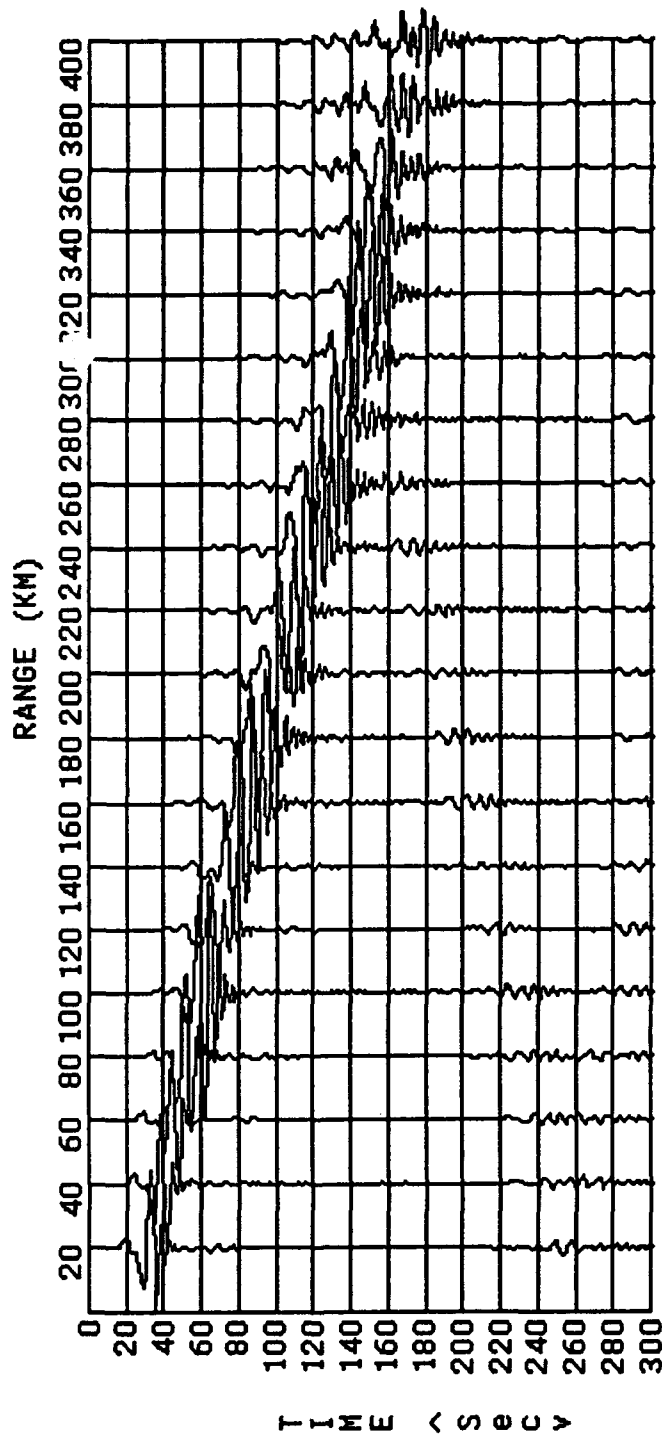


Figure 8-(e). The finite-element synthetic seismogram for the Basin and Crust-Pinch Model of Figure 3-(c), (basin width = 250 km, basin depth = 15 km, height of Moho-uplift = 10 km), with the basin velocity of 2.70 km/sec, as observed at distances of 20 km to 400 km by a source with a center frequency 0.167 Hz.

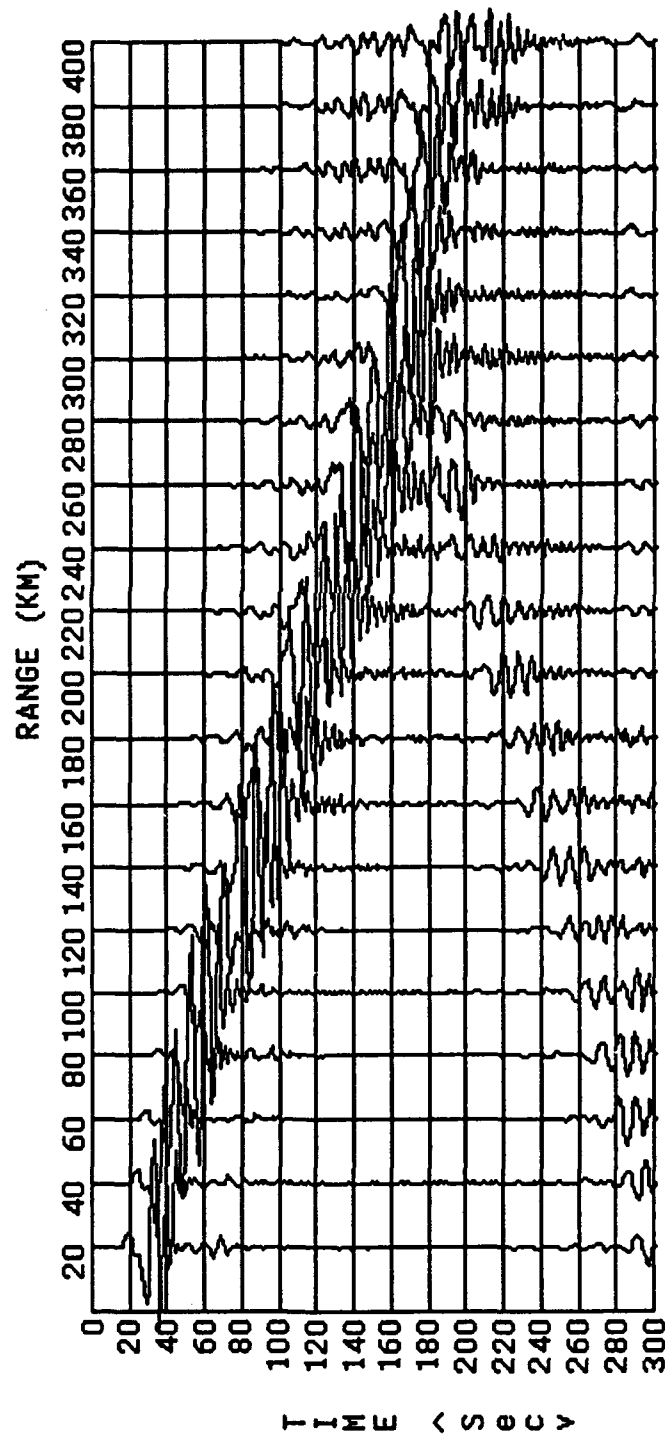


Figure 8-(f). The finite-element synthetic seismogram for the Basin and Crust-Pinch Model of Figure 3-(c), (basin width = 250 km, basin depth = 15 km, height of Moho-uplift = 10 km), with the basin velocity of 2.20 km/sec, as observed at distances of 20 km to 400 km by a source with a center frequency 0.167 Hz.

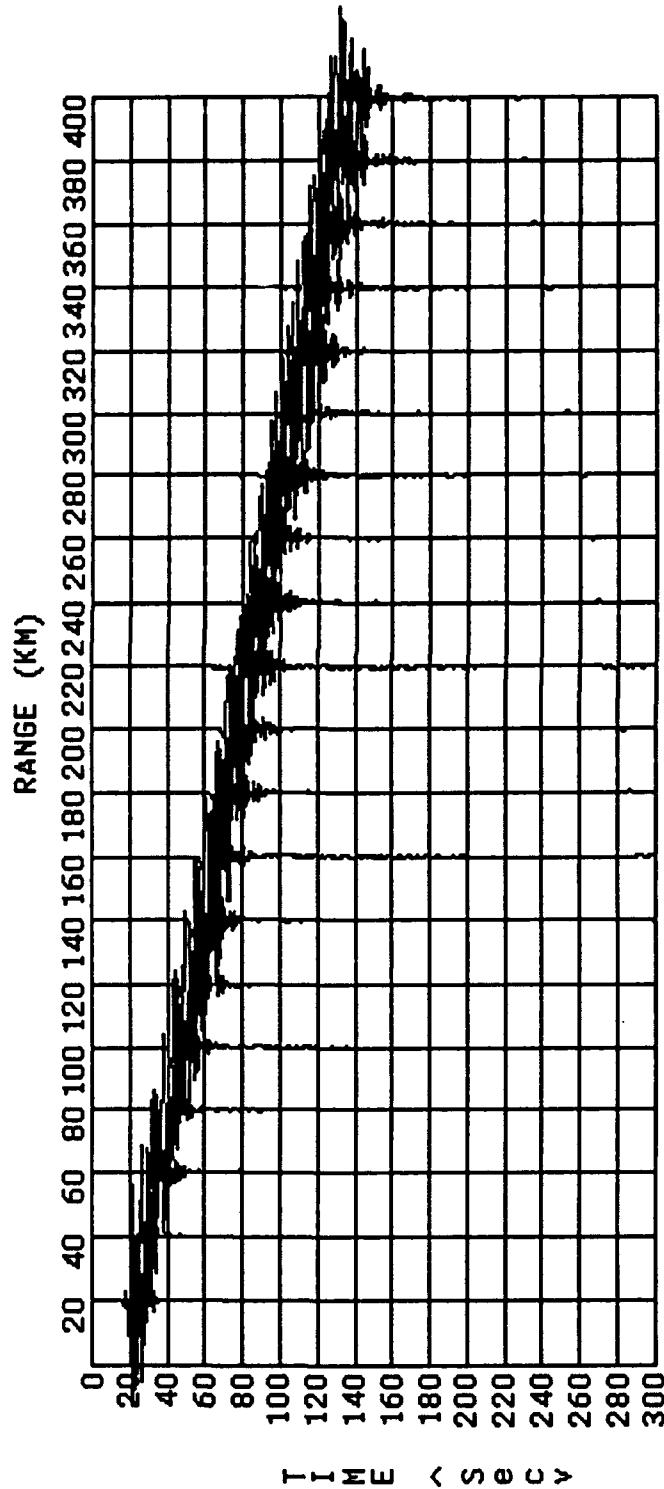


Figure 9-(a). The finite-element synthetic seismogram for the Basin Model of Figure 3-(b), (basin width = 250 km, basin depth = 15 km), with the basin velocity of 3.51 km/sec, as observed at distances of 20 km to 400 km by a source with a center frequency 0.667 Hz. (the basin is replaced by averaged granitic/basaltic material, i.e. no basin.)

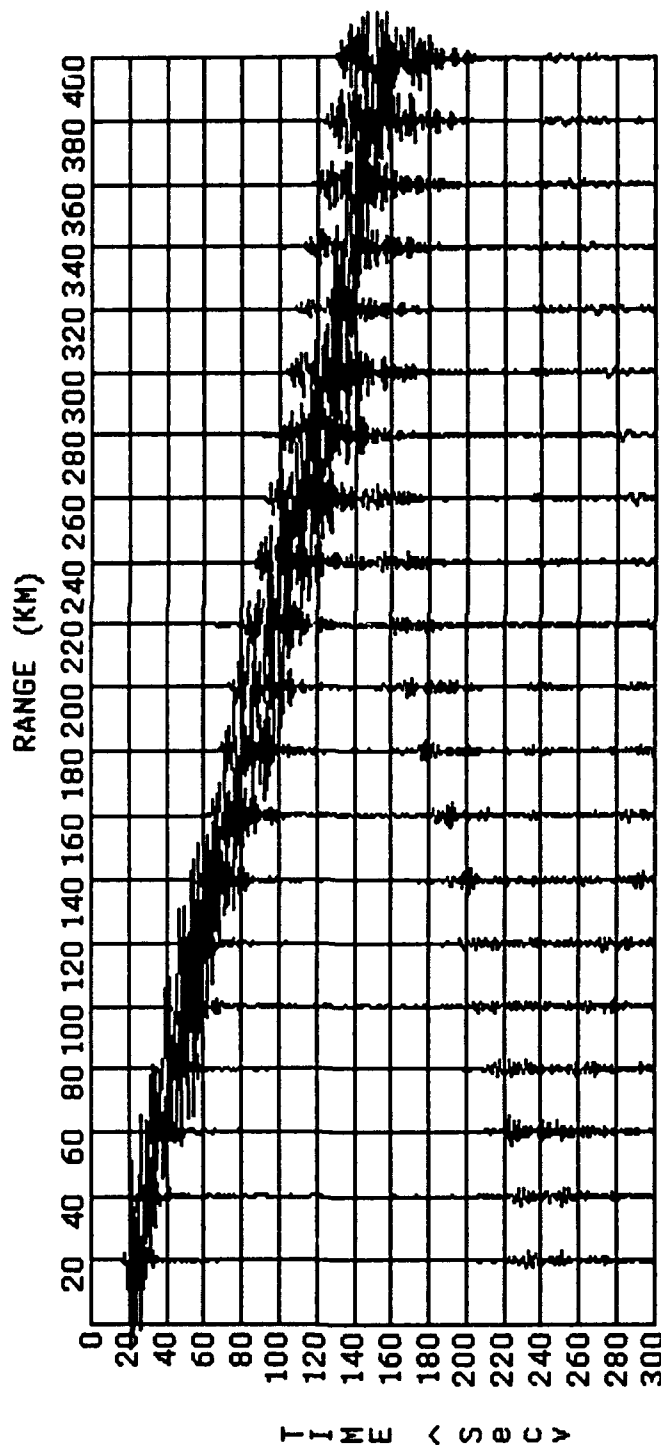


Figure 9-(b). The finite-element synthetic seismogram for the Basin Model of Figure 3-(b), (basin width = 250 km, basin depth = 15 km), with the basin velocity of 2.70 km/sec, as observed at distances of 20 km to 400 km by a source with a center frequency 0.667 Hz. (the basin is replaced by averaged granitic/basaltic material, i.e. no basin.)

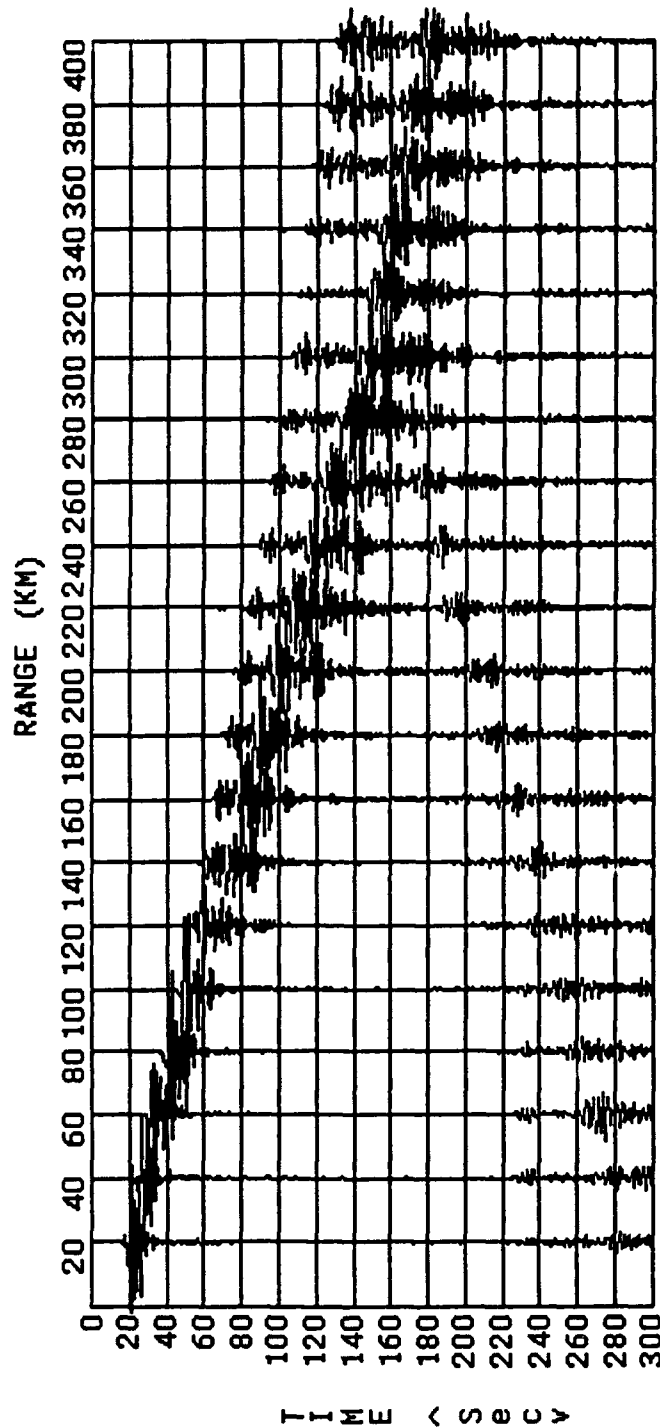


Figure 9-(c). The finite-element synthetic seismogram for the Basin Model of Figure 3-(b), (basin width = 250 km, basin depth = 15 km), with the basin velocity of 2.20 km/sec, as observed at distances of 20 km to 400 km by a source with a center frequency 0.667 Hz. (the basin is replaced by averaged granitic/basaltic material, i.e. no basin.)

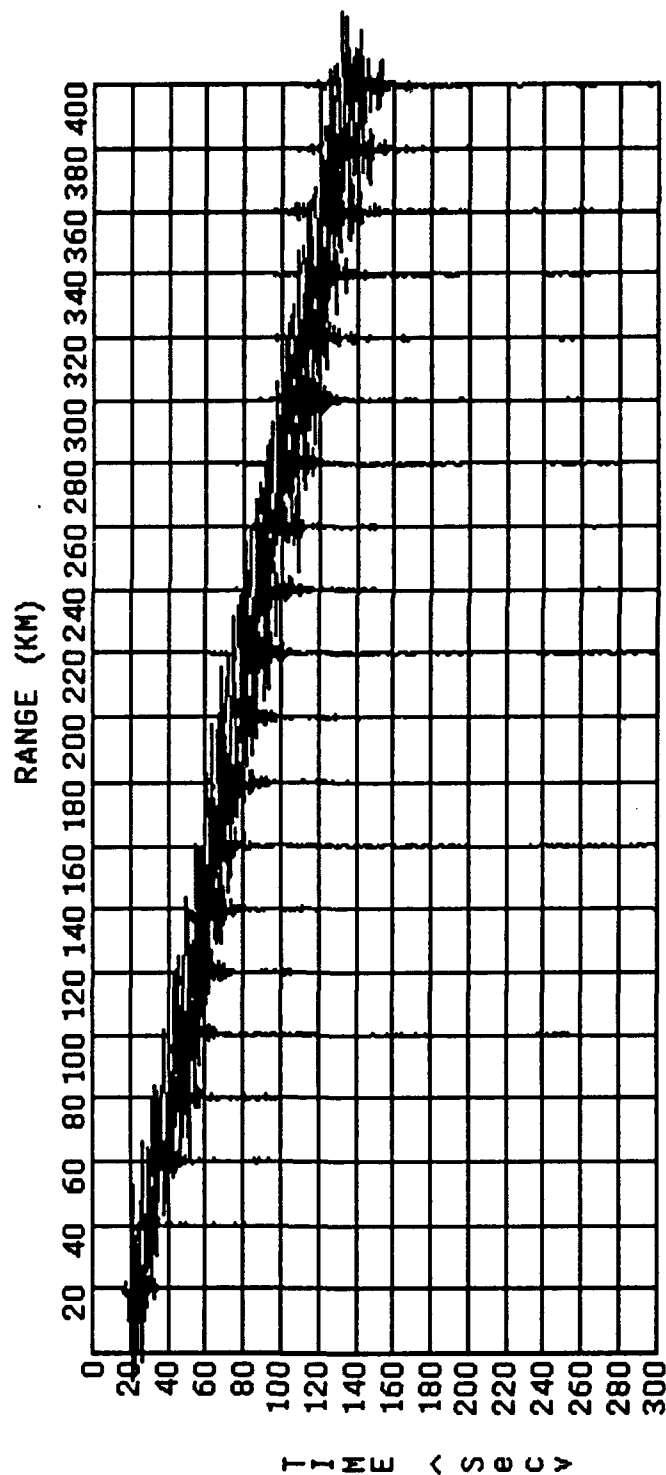


Figure 9-(d). The finite-element synthetic seismogram for the Basin and Crust-Pinch Model of Figure 3-(c), (basin width = 250 km, basin depth = 15 km, height of Moho-uplift = 10 km), with the basin velocity of 3.51 km/sec, as observed at distances of 20 km to 400 km by a source with a center frequency 0.667 Hz (no basin).

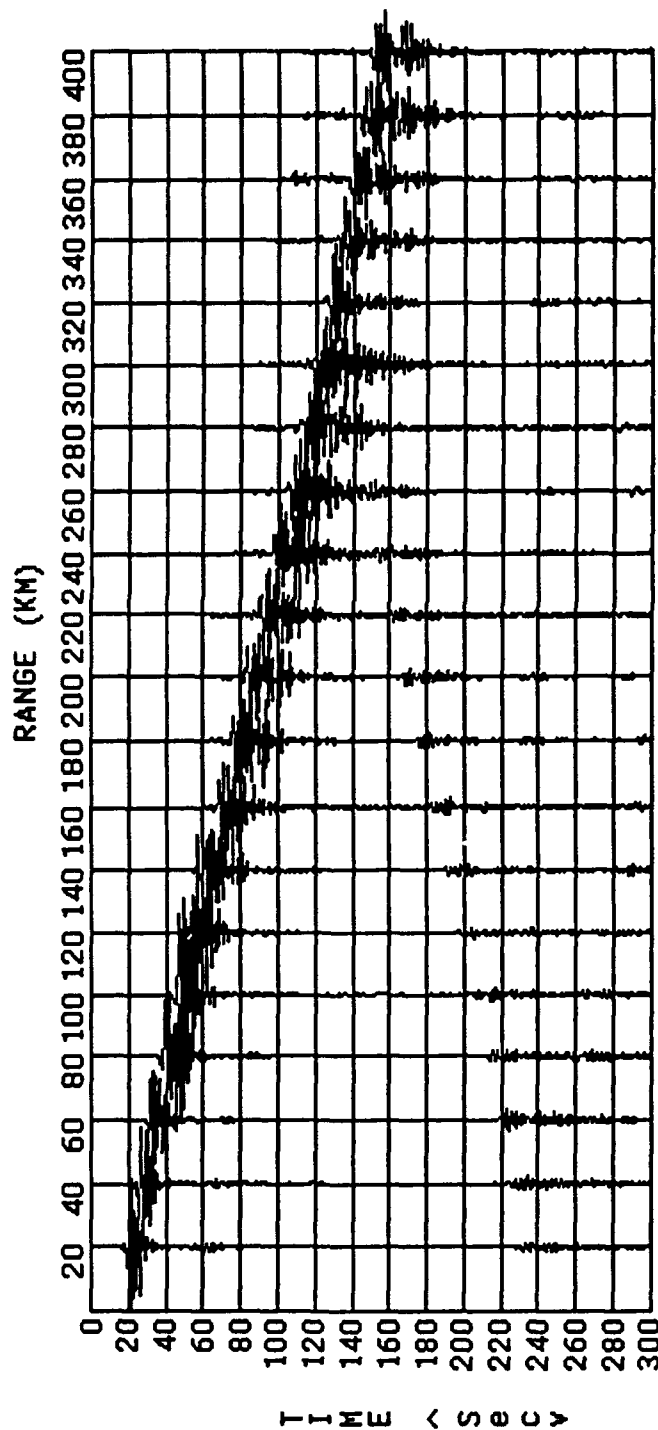


Figure 9-(e). The finite-element synthetic seismogram for the Basin and Crust-Pinch Model of Figure 3-(c), (basin width = 250 km, basin depth = 15 km, height of Moho-uplift = 10 km), with the basin velocity of 2.70 km/sec, as observed at distances of 20 km to 400 km by a source with a center frequency 0.667 Hz.

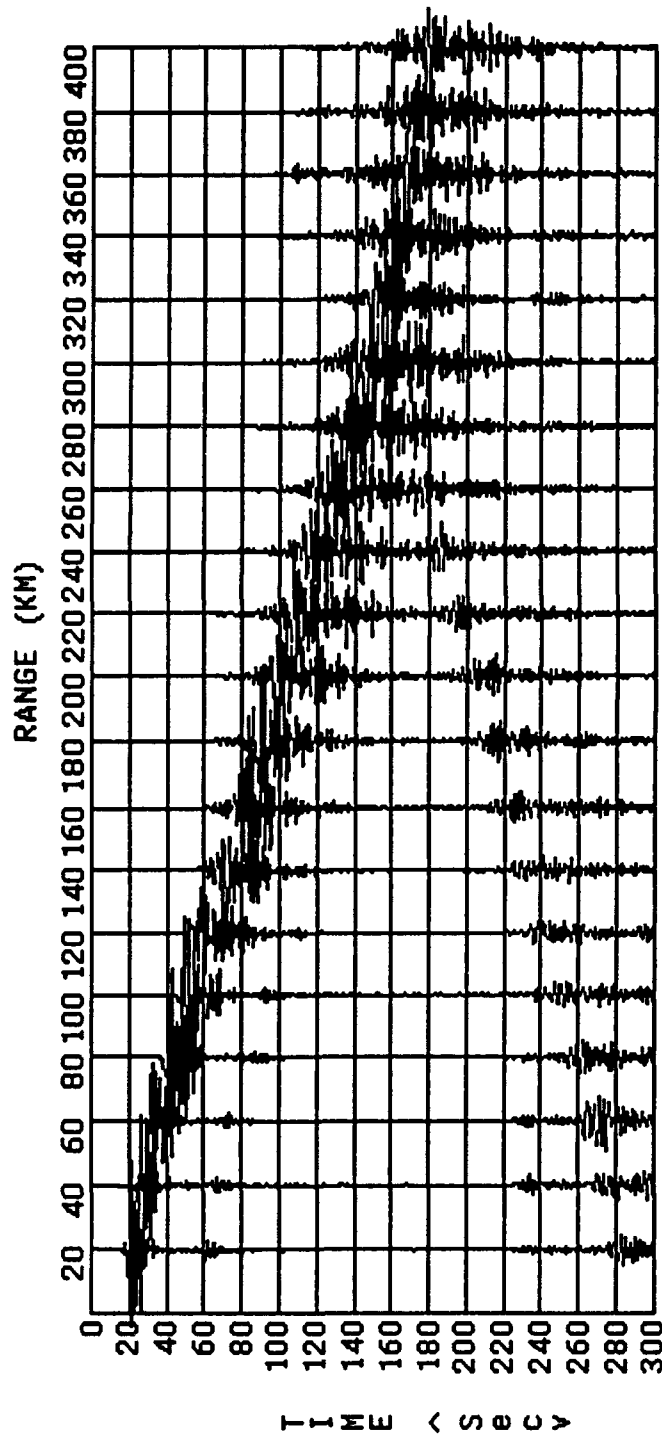


Figure 9-(f). The finite-element synthetic seismogram for the Basin and Crust-Pinch Model of Figure 3-(c), (basin width = 250 km, basin depth = 15 km, height of Moho-uplift = 10 km), with the basin velocity of 2.20 km/sec, as observed at distances of 20 km to 400 km by a source with a center frequency 0.667 Hz.

REFERENCES

1. Alford, R.M., K.R. Kelly, and D.M. Boore (1974). Accuracy of finite difference modelling of the acoustic wave equation, *Geophysics*, **39**, 834-842.
2. Bath, M., (1954). The elastic waves Lg and Rg along Euro-asiatic paths, *Ark. Geofys.*, **2**, 295-324.
3. Baumgardt, D.R., (1985). Comparative analysis of teleseismic P coda and Lg waves from underground nuclear explosions in Eurasia, *Bull. Seism. Soc. Am.*, **75**, 1413-1433.
4. Baumgardt, D.R., (1987). Spectral determination of regional and teleseismic Lg attenuation and source multiplicity in explosions, DARPA/AFGL Seismic Research Symposium, 15 - 18 June 1987, Harbor House, Nantucket, MA.
5. Baumgardt, D.R., (1990a). Investigation of teleseismic Lg blockage and scattering using regional arrays, *Bull. Seism. Soc. Am.*, **80**, 2261-2281.
6. Baumgardt, D.R., (1990b). Causes of Lg amplitude variations and scattering in the Eurasian continental craton, *Proceedings of the 12th Annual DARPA/AFGL Seismic Research Symposium*, 18 - 20 Sept., 1990, 224-233.
7. Bouchon, M., (1982). The complete synthesis of seismic crustal phases at regional distances, *J. Geophys. Res.*, **87**, 1735-1741.
8. Cara M. and J.B. Minster, (1981). Multi-mode analysis of Rayleigh-type Lg, Part 1. Theory and applicability of the method, *Bull. Seism. Soc. Am.*, **71**, 973-984.
9. Cao S. and K.J. Muirhead, (1993). Finite difference modelling of Lg blockage, *Geophys. J. Int.*, **115**, 85-96.
10. Cara, M. J.B. Minster, and R. LeBras, (1981). Multi-mode analysis of Rayleigh-type Lg, Part 2. Application to southern California and the northwestern Sierra Nevada, *Bull. Seism. Soc. Am.*, **71**, 985-1002.
11. Chan, W.W. and B. J. Mitchell (1985). Surface wave dispersion, crustal structure, and sediment thickness variations across the Barents shelf, *Geophys. J. R. Astron. Soc.*, **80**, 329-344.
12. Clarke, J.W. and J. Rachlin (1990). Geology of the Barents Sea Structural Basin. U.S. Geological Survey, Military Geology Project, Open-File Report, July, 1990.
13. Fan, Z.X. and Y.C. Teng (1989). The application of simulation modeling of seismic wave in the transversely isotropic and viscoelastic media, *Bull. of Chinese Geophys. Soc., Applied Geophys.*, **1**, 37-56.
14. Gramberg, I.S., (1988). The Barents Shelf Plate (in Russian), Volume 196, Nedra, Leningrad.
15. Hassanzadeh, S., (1985). Automatic three-dimensional mesh generation, Tech. memo., Chevron Oil Field Research Co., La. CA.
16. Hassanzadeh, S., Y.C. Teng, and J.T. Kuo (1987). Computation of wave fields in fluid-saturated porous media, 57th Ann. Internal. Mtg., Soc. Explor. Geophys., Expanded Abstract, 293-296.
17. Hughes, T.J.R. (1987). *The Finite-Element Method*, Prentice-Hall, Englewood Cliffs, N.J..
18. Kadinsky-Cade, K., M. Barazangi, J. Oliver, and B. Isacks (1981). Lateral variations of high-frequency seismic wave propagation at regional distances across the Turkish and Iranian Plateaus. *J. Geophys. Res.*, **86**, 9377-9396.

19. Kennett, B.L.N. (1986). Lg waves and structural boundaries, *Bull. seism. Soc.*, **76**, 1133-1141.
20. Kennett, B.L.N., S. Gregersen, S. Mykkeltveit, and S. Newmark (1985). Mapping of crustal heterogeneity in the North Sea basin via the propagation of Lg-waves, *Geophys. J. R. Astron. Soc.*, **83**, 299-306.
21. Kuo, J.T. and Y.C. Teng (1982). Ground response in alluvial basins due to seismic disturbances, AFGL-TR-82-0279.
22. Kuo, J.T. and Y.C. Teng (1984). Ground response in alluvial basins due to seismic disturbances, AFGL-TR-84-0104.
23. Kuo, J.T. and Y.C. Teng (1985). Ground response in alluvial basins due to seismic disturbances, AFGL-TR-85-0062.
24. Kuo, J.T., Y.C. Teng, C. Gong, and K.H. Chen (1975). Numerical and analytical solutions to elastodynamic problems, AFCRL-TR-75-0482.
25. Kuo, J.T., Y.C. Teng, K.H. Chen, and L.F. Huang (1977). Numerical and analytical solutions to elastodynamic problems, AFOSR-76-2908.
26. Kuo, J.T., Y.C. Teng, K.H. Chen, and C.E. Shepherd (1981). Elastic and viscoelastic wave scattering and diffraction, F49620-77-0130.
27. Knopoff, L., F. Schwab, K. Nakanishi, and F. Chang (1975). Evaluation of Lg as a Discriminant among Different Continental Crustal Structures, *Geophys. J. R. Astron. Soc.*, **39**, 41-70.
28. Marfurt, K.J. (1980). Finite-element modeling of seismic wave propagation, PROJECT MIDAS Annual Report I, 27-80.
29. Marfurt, K.J. (1984). Accuracy of finite-difference and finite-element modeling of the scalar and elastic wave equations, *Geophysics*, **49**, 533-549.
30. Marshall, G., P. Eiseman, and J.T. Kuo, A general collapsing technique for three-dimensional algebraic grid generation, *J. Comput. Phys.* **61**, 180-198.
31. Nuttli, O.W. (1973). Seismic wave attenuation and magnitude relations for eastern North America, *J. Geophys. Res.* **78**, 876-885.
32. Mitchell, B.J. and H.J. Hwang (1987). Effect of low-Q sediments and crustal Q on Lg attenuation in the United States. *Bull. Seism. Soc. Am.*, **77**, 1197.
33. Ni, J. and M. Barazangi (1983). High-frequency seismic wave propagation beneath the Indian Shield, Himalayan Arc, Tibetan Plateau and surrounding regions: high uppermost mantle velocities and efficient Sn propagation beneath Tibet. *Geophys. J. R. Astron. Soc.*, **72**, 665-689.
34. Oliver, J. and M. Ewing, (1957). Higher modes of continental Rayleigh waves, *Bull. Seism. Soc. Am.*, **47**, 187-204.
35. Oliver, J. and M. Ewing, (1958a). Normal modes of continental surface waves, *Bull. Seism. Soc. Am.*, **48**, 33-49.
36. Oliver, J. and M. Ewing, (1958b). The effect of surficial sedimentary layers on continental surface waves, *Bull. Seism. Soc. Am.*, **47**, 339-354.
37. Panza, G.F., and G. Calcagnile (1975). Lg, Li and Rg from Rayleigh modes, *Geophys. J. R. Astron. Soc.*, **40**, 475-487.
38. Piwinskii, A.J. (1981). Deep structure of the earth's crust and upper mantle in the USSR according to geological, geophysical, and seismological data: Dneiper-Donetsk and Pri-Caspoan depressions, UCID-19203, Lawrence Livermore Laboratory, Livermore, California.
39. Press, F. and M. Ewing, (1952). Two slow surface waves across North America, *Bull. Seism. Soc. Am.*, **42**, 219-228.

40. Regan, J., and D.G. Harkrider, (1989). Numerical modelling of SH Lg waves in and around continental margins, *Geophys. J. Int.*, bf 98, 107-130.
41. Ruzaiкин, A., I. Nersesov, V. Khalturin, and P. Molnar (1977). Propagation of Lg and lateral variations in crustal structure in Asia. *J. Geophys. Res.*, 82,307-316.
42. Teng, Y.C. (1981). Preliminary version of the Aldridge finite-element algorithm for three dimensions, AFEA.3, Project MIDAS Annual Report II, 333-386.
43. Teng, Y.C. (1982). A finite-element algorithm for solving the dynamic problem of a fluid-solid interface, Project MIDAS Annual Report III, 55-71.
44. Teng, Y.C. (1988). finite-element algorithms for multiple array processors, Proceedings, 12th IMACS World Congress, Paris, France, Expanded Abstract, 241-243.
45. Teng, Y.C. (1989). Three-dimensional finite-element analysis of waves in acoustic media with inclusion, *J. Acoust. Soc. Am.*, 86, 414-422.
46. Teng, Y.C. (1990). Finite-element results of the slow compressional wave in a porous medium at ultrasonic frequencies, *J. Appl. Phys.* 68, 4335-4337.
47. Teng, Y.C. (1993). Scattering of transient waves by finite cracks in an anti-plane strain elastic solid, *J. of Compu. Acou.*, bf 1, No.1, 101-116.
48. Teng, Y.C. and T.F. Dai (1989). Finite-element prestack reverse-time migration for elastic waves, *Geophysics*, 54, 1204-1208.
49. Teng, Y.C. and J.T. Kuo (1982). Improved version of the Aldridge three-dimension finite-element algorithm, AFEA3.A, Project MIDAS Annual Report III, 20-54.
50. Teng, Y.C. and J.T. Kuo (1983). Updated version of the Aldridge three-dimension elastodynamic finite-element code, AFEA3.B, Project MIDAS Annual Report IV, 1-39.
51. Teng, Y.C. and J.T. Kuo (1984). Finite-element source simulation, Project MIDAS Annual Report V, 272-308.
52. Teng, Y.C. and J.T. Kuo (1988a). finite-element source simulation for elastodynamics, *Model Optimization in Exploration Geophysics*, Vol. 3, Vieweg Braunschweig-Wiesbaden, 277-298.
53. Teng, Y.C. and J.T. Kuo (1988b). A finite-element algorithm for solving the transient problem in a fluid-solid coupled medium, IMACS, COMPU. ACOU.: Wave Propagation, 239-257.
54. Teng, Y.C. and Z.L. Zhang (1990). Three-dimensional modelling of elastic waves, *Acta Geophysica Sinica*, 33, n.1, 44-53.
55. Teng, Y.C., T.F. Dai, and J.T. Kuo (1986). Finite-element reverse-time migration for elastic waves, 56th Ann. Internal. Mtg., Soc. Explor. Geophys., Expanded Abstract, 611-614.
56. Teng, Y.C., T.F. Dai, and J.T. Kuo (1988). Pre-stack finite-element reverse-time migration for elastic waves, *Geophysical Prospecting for Petroleum (PRC)*, 27, n.2, 10-26.
57. Zienkiewicz, O.C. (1977). *The Finite Element Method*, McGraw-Hill Book Co., New York, London.

COLUMBIA UNIVERSITY
INTERDEPARTMENT MEMORANDUM

Date_____

To_____

Subject_____

Approved for public release;
distribution unlimited.

AIR FORCE OF SCIENTIFIC RESEARCH (AFSC)
NOTICE OF TRANSMITTAL TO DTIC
This technical report has been reviewed and is
approved for public release IAW AFR 190-12
Distribution is unlimited.
Joan Boggs
STINFO Program Manager